ELSEVIER

Journal of Volcanology and Geothermal Research 115 (2002) 53–82

Journal of volcanology and geothermal research

www.elsevier.com/locate/jvolgeores

Ohaaki reservoir chemistry: characteristics of an arc-type hydrothermal system in the Taupo Volcanic Zone, New Zealand

B.W. Christenson [a,*], E.K. Mroczek [a], B.M. Kennedy [b], M.C. van Soest [b], M.K. Stewart [c], G. Lyon [c]

[a] *Institute of Geological and Nuclear Sciences, Private Bag 2000, Taupo, New Zealand*
[b] *Lawrence Berkeley National Laboratory, Berkeley, CA, USA*
[c] *Institute of Geological and Nuclear Sciences, Private Bag, Lower Hutt, New Zealand*

Received 9 October 2000; accepted 4 September 2001

Abstract

Situated along the eastern margin of the Taupo Volcanic Zone (TVZ), the high-gas and high-enthalpy production fluids from the Ohaaki geothermal field are chemically similar to other arc-type volcanic systems found along this part of the TVZ. Two thermal upwellings can be distinguished within the field, each apparently emanating from fault structures in the Mesozoic basement greywackes. Although both plumes have similar salinities and appear to be fully equilibrated with the reservoir rocks containing them, fluids associated with the eastern upflow zone are enriched in B and F compared to those in the western upflow zone. δ^2H and $\delta^{18}O$ signatures for water suggest that up to 20% of the water in the discharges may derive from a magmatic source, and a δ^2H–Cl trend established by the East-Bank fluids indicate end-member mixing between a high-Cl fluid and Cl-deficient steam containing as much as 40% arc-type vapour. Gas signatures in fluids from the two production fields show compositional differences that cannot be explained by physical reservoir processes. The eastern fluids have higher N_2/Ar and CO_2/He ratios, and consistently higher CH_4–CO_2 ^{13}C fractionation temperatures than those in the western upflow zone. In addition, stark differences in $^3He/^4He$ and $^{40}Ar/^{36}Ar$ ratios for the two production fields suggest two-component mixing for the respective source components, with the eastern fluids having a significantly larger radiogenic gas content than those to the west. Collectively, these signatures suggest the presence of a relatively young and shallowly seated degassing intrusive beneath the eastern upflow zone, perhaps as shallow as 4 km beneath the surface.

Keywords: geothermal; magmatic heat sources; magmatic degassing; fluid chemistry; noble gas chemistry

1. Introduction

The depths and chemical characteristics of heat sources which drive TVZ geothermal systems are generally poorly understood. This is due in part to the deepest geothermal wells in the TVZ having

* Corresponding author. Tel.: +64-7-374-8211; Fax: +64-7-374-8199.
E-mail address: b.christenson@gns.cri.nz (B.W. Christenson).

0377-0273/02/$ – see front matter
PII: S0377-0273(01)00309-2

penetrated to just 2800 m below surface, and in only one of these wells (NM4 at Ngatamariki, Fig. 1) has an igneous intrusive body been intersected (Browne et al., 1992; Christenson et al., 1998). At Kawerau there is a clear indication that the present-day heat source relates to young volcanism within the field (Christenson, 1997). However, being at the margins of the explored reservoir, little is presently known of the characteristics of that heat source.

It is widely acknowledged that the high heat flow in the TVZ is fostered by extensional tectonism related to westerly dipping subduction beneath the North Island (e.g. Cole, 1990; Stern, 1987). Theoretical heat transfer models have been proposed which attempt to fit the observed heat flow at the surface (Weir, 2000) and distribution of geothermal systems across the TVZ (McNabb, 1992; Kissling, 1997). All of these models assume the presence of a granitic batholith at depths of ca. 8 km beneath much of the TVZ, with the geothermal systems being a natural consequence of stable convective flow regimes over this heat source.

Giggenbach (1995), however, recognised that the gases discharged from geothermal systems along the eastern margin of the TVZ (e.g. Kawerau, Ohaaki, Waiotapu, Rotokawa) have close affinities to those discharged from TVZ andesitic volcanoes, and with active arc-type volcanoes elsewhere in the world. This observation is consistent with the view that present-day arc magmas are generated along the eastern margin of the TVZ (cf. Cole, 1990), but more importantly, it

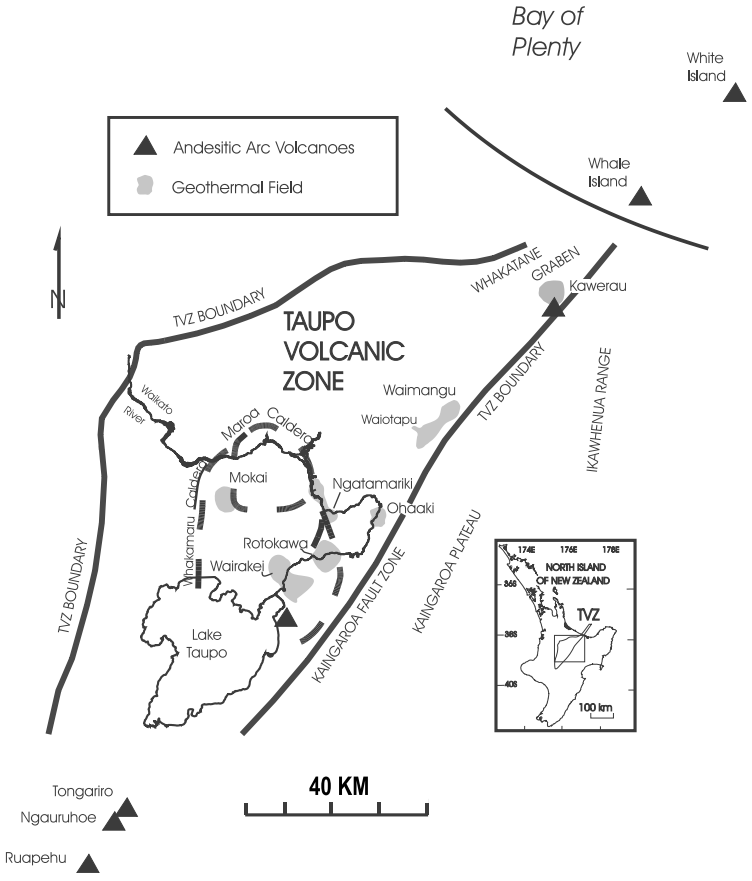

Fig. 1. Map of the TVZ, showing distribution of some of the geothermal fields as denoted by their resistivity signatures, with emphasis on the arc-type systems occurring along the eastern margin.

indicates that subsurface arc-type magmatic systems exist in the TVZ where there is presently no surface expression of recent volcanism. The occurrence of a shallow intrusive in the Ngatamariki geothermal field (Browne et al., 1992; Christenson et al., 1998), raises the possibility that some of the magmatic heat sources along the eastern TVZ may exist at considerably shallower depths than those residing in the marginal basin to the west.

The hydrothermal system at Ohaaki is of particular interest in this regard. The field, which came into production in 1989, has experienced substantial exploitation effects (draw-down, scaling and subsidence) as a result of the current New Zealand practice of relatively shallow-reservoir production. In 1995, the field operators (Contact Energy) undertook a deep exploration drilling programme seeking a more sustainable steam supply for the field. The objective was to locate production in the basement greywacke through the drilling of deep, highly deviated wells in order to mitigate the exploitation effects observed at shallower levels of the reservoir. Although the results of the drilling were somewhat disappointing from a production–permeability standpoint, higher than expected reservoir pressures were encountered in the eastern part of the field, and have in part been the motivation for the current study.

It is in this context that we re-assess the geochemical structure of the Ohaaki system in light of what we know of New Zealand's magmatic–hydrothermal environments (e.g. Giggenbach, 1974, 1987; Christenson and Wood, 1993; Christenson, 2000), the structure and evolution of the TVZ (Cole, 1990; Stern, 1987), and the experience of deep geothermal exploration elsewhere in the world (e.g. Kakkonda, Muraoka et al., 1998; the Geysers, Donnelly-Nolan et al., 1993; Kennedy and Truesdell, 1996), with a view to characterising the heat source(s) for the system. We present results of a comprehensive geochemical study of current production discharges in the field, and integrate these results with previous findings to create a picture of the nature and location of the current heat source(s) for the system. The aim is to provide not only a conceptual model for the field which will assist with future exploration/production drilling, but also to shed some light on the characteristics of arc-type hydrothermal systems in the TVZ.

2. Sampling and analysis

Fluids were sampled from a total of 23 wells from both East- and West-Bank production fields (Fig. 2) between 1997 and 1999. In most cases, fluids were sampled from two-phase production lines using a Webre separator, although only cold bleed-line gases were available from some wells. Liquid-phase samples collected at >100°C

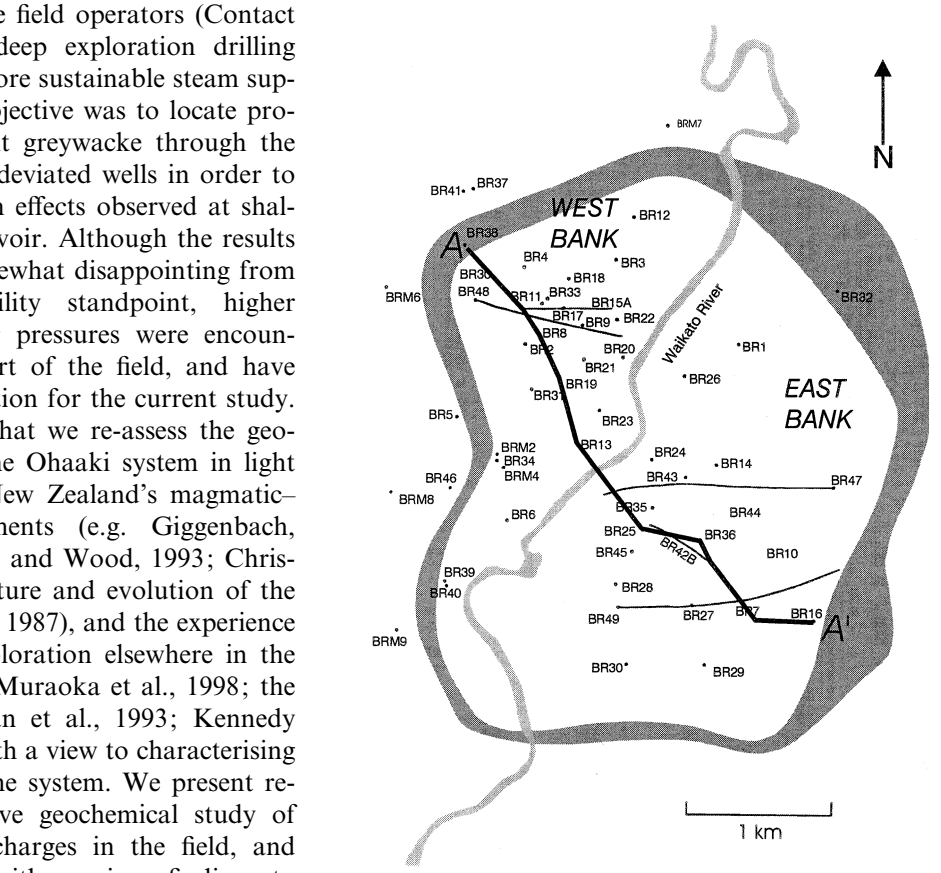

Fig. 2. Map of the Ohaaki borefield. Shaded boundary reflects the 20–50-Ωm signature at 1000 m depth (Risk, 1993). Black lines represent the traces of recently drilled deviated production wells, and the line marked A–A′, represents the line of section portrayed in Fig. 3.

were passed through a cooling coil, and collected at temperatures typically $<30°C$. A series of water/gas samples were taken for analysis including a 500-ml raw sample, a 200-ml sample filtered to 0.45 μm and acidified to ca. pH 2, a sample for dissolved gases, a 500-ml sample taken into acid-washed plastic containers for trace metal analysis, and 12-ml water samples taken into glass bottles for ^{2}H and ^{18}O analysis.

Waters were analysed by a variety of techniques. Cations (including B and SiO_2) were analysed by ICP–OES and AAS, whereas anions were measured by ion chromatography (F, Cl and Br), potentiometry (Cl) and titrimetry (HCO_3^-). pH was measured by glass electrode calibrated at pH 4.0 and 7.0.

Steam samples were collected into evacuated flasks filled with 50 ml of 6 N NaOH. Condensed steam was collected into evacuated flasks for NH_3 analysis, and into 12-ml glass bottles for ^{2}H and ^{18}O analysis. Splits of the non-condensable gases for noble gas isotope analysis were taken from these flasks into He diffusion-resistant breakseal glass tubes (Dow-Corning 8250 glass). Gases were analysed by a combination of gas chromatography and wet chemical means following essentially the methods laid out in Giggenbach and Goguel (1989). Noble gases were analysed at Lawrence Berkeley National Laboratory on the RARGA facility following the methodology described in Kennedy et al. (1985).

Deuterium and ^{18}O analyses were carried out by equilibrating the water with hydrogen and carbon dioxide gas, respectively, at 30°C. The gases were then analysed by stable isotope mass spectrometry following the method of Hulston et al. (1981). Results are reported in delta notation relative to VSMOW where

$$\delta^2H = \left(\left(^2H/H\right)_{sample}/\left(^2H/H\right)_{VSMOW} - 1\right) \times 1000\,‰$$

and similarly for $\delta^{18}O$. Standard deviations of the measurements are typically $\pm 1.0‰$ and $\pm 0.1‰$, respectively. Carbon isotopes on CH_4 and CO_2 were analysed following the method of Lyon and Hulston (1984), with standard deviations of $\pm 0.1‰$.

3. Thermal, chemical and isotopic signatures of reservoir waters

3.1. Measured reservoir temperatures

The NW–SE cross-section indicated in Fig. 2 is shown in Fig. 3. This profile is similar to that presented in Hedenquist (1990), but updated with measurements from new wells. The Mesozoic basement greywackes are displaced along normal faults which coincide with two thermal upwellings, one beneath each of the current production fields. Maximum measured temperatures in the field were measured on the West Bank in well 34 (310°C at 2580 m). The thermal gradients are somewhat steeper on the West Bank than on the East Bank, particularly in the temperature interval of 275°C to 300°C. The maximum temperature on the East Bank is in well 47 (302°C, close to the point of intersection of the well with the plane of section in Fig. 3). The position of the contour of 300°C under wells 36 and 42 in Fig. 3 is not rigorously constrained by measured temperatures but is consistent with geochemical data from production fluids (see below). The maximum

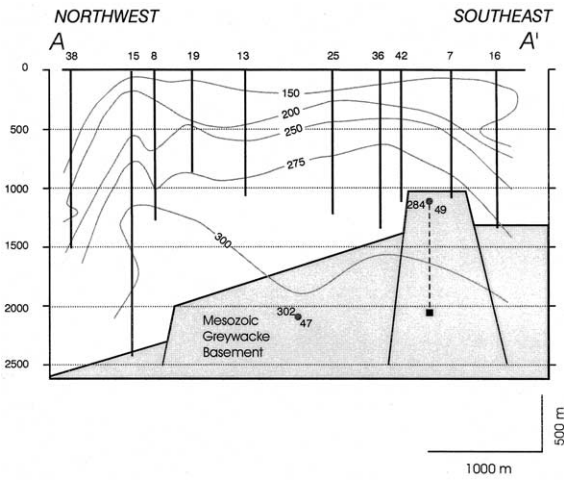

Fig. 3. Cross-section through the Ohaaki reservoir showing measured temperatures and major structures which offset the basement greywackes. Points labelled 49 and 47 show the intersections of these wells with the plane of section, their respective measured temperatures, and in the case of 49 the projected location of the bottom of the well (filled square).

Table 1
Composition of waters discharged from production wells at Ohaaki between 1997 and 1999

Well	Date	CP	TA	pH	Li	Na	K	Ca	Mg	Rb	Cs	Cl	SO_4	B	SiO_2	HCO_3	H_2S_D	NH_{3D}	Br	F	As	$\delta^{18}O_{wat}$ (‰)	$\delta^{2}O_{wat}$ (‰)
8	10.4.97	3.6	18	7.45	8.1	682	76	9.6	0.49	0.61	0.71	634	88	17.7	303	924	12.0	1.4	2.2	3.8	1.3	−5.22	−39.8
10	1.5.99	10	19	5.87	6.6	672	78	1.2	0.04	0.64	1.07	894	14	33.0	430	790	7.6	14.0	2.9	3.3	0.3	na	na
14	5.5.99	6.8	22	6.85	6.6	736	89	5.9	0.01	0.84	0.97	1121	6	35.0	430	186	3.0	10.0	3.7	8.6	1.0	na	na
15	7.4.97	18.1	22	6.30	8.4	726	157	0.9	0.01	1.46	1.05	1170	9	30.1	699	678	16.0	6.0	3.9	5.4	2.9	−4.54	−39.0
18	13.7.99	3.8	18	7.13	6.9	849	160	3.3	0.01	1.20	1.10	1231	16	27.0	471	375	4.5	6.5	4.9	3.3	0.2	na	na
20	15.1.98	0	21	9.16	11.2	936	151	0.7	0.01	1.29	1.17	1197	79	36.4	760	460	5.6	1.6	4.0	5.4	2.6	−3.44	−36.9
20	25.2.98	8.3	23	8.44	9.7	772	123	0.5	0.01	1.07	0.99	1033	66	31.3	620	458	13.9	3.5	3.7	5.1	2.2	−4.47	−40.6
22	7.4.97	9.8	22	7.20	11.4	994	194	0.5	0.01	1.60	1.36	1606	21	46.8	546	427	8.0	6.0	5.1	6.4	3.4	−3.82	−38.9
24	17.3.98	6.9	20	6.92	7.9	799	140	5.7	0.01	1.17	1.27	1398	8	41.6	575	194	4.4	10.0	4.7	4.4	3.6	−3.67	−42.0
25	10.4.97	10.9	18	8.64	8.4	728	107	0.3	0.02	1.05	1.02	837	23	25.8	596	596	18.0	2.8	2.8	7.8	1.8	−4.46	−39.5
31	17.3.98	3.4	20	7.90	8.8	800	130	1.3	0.01	1.13	1.09	1116	43	33.4	584	340	11.0	3.8	4.1	5.5	2.8	−4.14	−42.2
36	19.1.98	0	21	8.66	11.2	1041	155	0.5	0.01	1.39	1.34	1408	10	58.6	790	428	5.8	2.3	4.6	10.8	3.7	−2.37	−26.4
36	26.2.98	8.7	23	7.78	9.4	788	128	0.5	0.01	1.13	1.07	1124	13	46.8	645	450	13.0	3.9	3.7	8.1	3.0	−3.99	−39.9
42	11.4.97	14.9	18	6.84	9.1	801	104	1.2	0.01	0.97	1.03	1144	13	48.9	482	450	11.0	6.5	3.7	8.4	2.7	−3.97	−39.6
43	26.2.98	10.5	18	7.24	9.2	745	136	0.6	0.05	1.40	1.18	1041	11	33.0	742	469	16.0	3.5	3.6	9.1	2.6	−4.42	−40.6
44	11.4.97	0	22	8.41	10.1	1014	148	3.0	0.01	1.26	1.38	1438	13	53.5	780	300	3.9	3.9	4.6	10.9	4.3	−2.45	−26.5
44	26.2.98	8.7	23	7.40	8.5	776	122	2.7	0.01	1.13	1.08	1195	15	43.8	645	324	8.4	5.7	4.0	8.8	3.5	−4.07	−39.8
48	7.3.97	5.7	24	7.05	9.8	847	177	3.5	0.10	1.63	1.42	1409	6	36.9	768	177	5.0	4.4	4.9	6.1	3.6	−3.96	−38.4
48	19.3.97	4.8	23	6.88	9.8	847	180	2.4	0.01	1.61	1.41	1414	5	35.7	788	205	5.9	4.0	5.3	5.8	3.6	−3.93	−36.4

Collection pressures (CP) are as bars gauge; concentrations, mg/l; TA, analysis temperature.

measured temperature in this area is 298°C in well 36. Although well 49 is much deeper than well 36, its deviated nature takes it on a track approximately parallel to the isotherms, and its maximum temperature is just 290°C.

3.2. Compositional characteristics of discharged waters

Analytical and isotopic data for the waters discharged from the production wells are listed in Table 1. The waters are of dilute alkaline-chloride composition, although as described by Hedenquist (1990), shallow fluids in the reservoir show evidence of steam heating, and consequently are relatively enriched in HCO_3^-. The discharge from well 8 shows elevated HCO_3, SO_4 and Mg contents, suggesting that there is a significant recharge component of steam-heated water in this production fluid.

3.2.1. Chloride–enthalpy relations

The relationship between heat and Cl content in the reservoir fluids is shown in Fig. 4, where reservoir Cl contents and liquid-phase enthalpies are calculated at the quartz equilibrium temper-

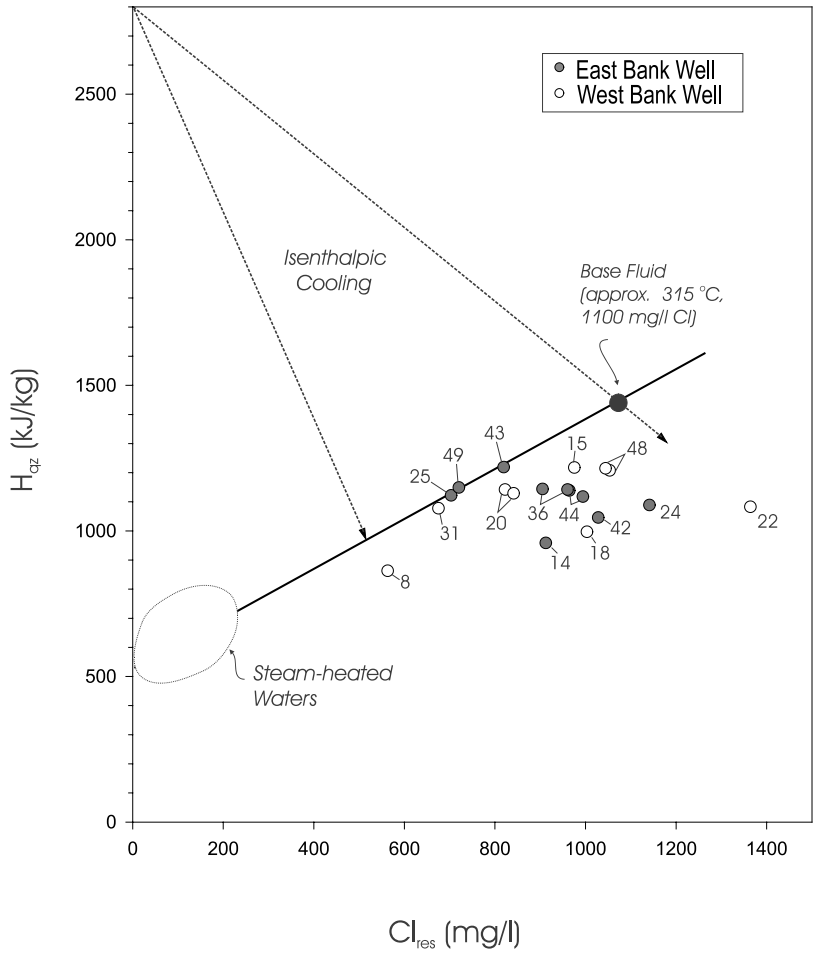

Fig. 4. Chloride–enthalpy diagram. Both Cl and enthalpy values have been calculated at the enthalpy of the reservoir liquid phase as determined by the quartz solubility temperature. The system mixing line extends to a field of dilute, steam-heated waters which have been demonstrated to be the primary diluent in the reservoir (Hedenquist, 1990). The least dilute fluid is produced from well 22, for which a base fluid temperature of 315°C and Cl content of 1100 mg/l have been calculated.

Table 2
Derived reservoir parameters for Ohaaki discharges

Well	P_{spl}	H_m	H_{qz}	Y_{Hm}	Y_{exh}	T_{qz}	Cl_{res}
8	3.6	958	863	0.16	0.05	202	563
14	6.8	2438	959	0.84	0.80	223	912
15	18.1	1317	1218	0.22	0.06	278	975
18	3.8	1588	997	0.45	0.33	231	1003
20	0	1095	1142	0.32	0.00	261	822
20	8.3	1095	1129	0.19	0.00	259	841
22	9.8	1242	1083	0.23	0.09	249	1364
24	6.9	1592	1089	0.43	0.29	251	1141
25	10.9	1059	1122	0.16	0.00	257	703
31	3.4	1157	1078	0.25	0.05	248	675
36	0	1749	1139	0.59	0.37	261	964
36	8.7	1749	1144	0.49	0.37	262	905
42	14.9	2155	1046	0.67	0.63	242	1028
43	10.5	991	1219	0.22	0.00	277	819
44	0	1970	1118	0.69	0.51	257	994
44	8.7	1970	1142	0.60	0.50	261	960
48	5.7	1575	1208	0.43	0.23	275	1053
48	4.8	1422	1215	0.36	0.13	276	1044
49	10.7	2134	1149	0.76	0.60	263	720

P_{spl}, sampling pressure (bg); H_m, measured enthalpy (kJ/kg); H_{qz}, enthalpy at the quartz equilibrium temperature; Y_{Hm}, vapour fraction at the measured enthalpy; Y_{exh}, excess vapour fraction; T_{qz}, quartz equilibrium temperature (°C); Cl_{res}, Cl concentration (mg/l) at T_{qz}.

atures (Table 2). The maximum enthalpy of the reservoir liquid phase calculated in this way is 1219 kJ/kg (277°C) in fluid from well 43. A system mixing line can be established for the system by projecting a line from this discharge to a steam-heated component of nil Cl content (at approximately 520 kJ/kg, cf. Hedenquist, 1990).

Using this mixing line as a reference, compositional variations due only to mixing of the source fluid with the end-member diluent can be ascertained. Changes in heat content and composition due to vapour loss in the reservoir can be corrected by projecting the discharge compositions back to the system mixing line along lines connecting reservoir compositions to the appropriate steam enthalpy.

This treatment shows that there is significant adiabatic cooling of most of the reservoir fluids, with discharges from wells 42, 24 and 22 being most affected by this process. It is also arguable from Fig. 4 that the West-Bank fluids have the highest Cl contents in the system, a fact which led earlier investigators (Mahon and Finlayson, 1977; Hedenquist, 1990) to conclude that the current heat source for the system lay under the West Bank. In their respective models, the main upflow for the field was in the vicinity of well 15, with outflow and mixing towards the east.

3.2.2. Stable isotopic signatures of water

The $\delta^{18}O$ and $\delta^{2}H$ isotopic characteristics of the production waters are portrayed in Fig. 5, where they are compared to the worldwide meteoric water line, local groundwater and Waikato River water (Stewart, 1978a), and to a reasonably complete set of production and monitor well data from 1990 (Stewart, 1992). The fluids are enriched by up to 3‰ in $\delta^{18}O$, and up to 6‰ in $\delta^{2}H$ over local groundwater compositions. ^{18}O enrichment is common in TVZ geothermal systems, and has been variously explained as the result of water–rock interactions (Stewart, 1978b; Blattner, 1985), and magmatic inputs (Hedenquist and Browne, 1989; Christenson, 1989). ^{2}H enrichment has been previously recognised in geothermal systems associated with arc-type volcanism (Taran et al., 1989), including Ohaaki and several other systems in the TVZ (Giggenbach, 1992).

Using ^{2}H as a tracer, it is possible to estimate the proportion of arc-type water (hereafter ATW) in geothermal discharges by assuming simple two-component mixing between local meteoric water (average $\delta^{18}O \approx -7.2$, $\delta^{2}H \approx -46$) and the inferred ATW composition of $\delta^{2}H = -20$, $\delta^{18}O = +10$ (Giggenbach, 1992). In the case of Ohaaki, the mean $\delta^{2}H$ value of $-41.5‰$ equates to 17% ATW, whereas the maximum $\delta^{2}H$ of $-40.3‰$ (from well 15) indicates some 22% ATW in the discharges. There is little distinction in the range or maximum values of $\delta^{2}H$ between the two production fields, although the trends exhibited by the data are of interest when considered in conjunction with heat- and mass-flows in the system (see below).

There is a positive correlation between Cl and ^{18}O contents for the production fluids from both production fields (Fig. 6a), suggesting reservoir mixing between a high-Cl, ^{18}O-enriched fluid, and a dilute, ^{18}O-depleted fluid (zero Cl and $\delta^{18}O$ of -5 to $-6‰$). The inferred end-member diluent signature is some 1.5–2‰ heavier than local meteoric water, suggesting that perhaps partial isotopic equilibration with reservoir rocks could produce the observed trend in $\delta^{18}O$ (e.g. Blattner, 1985). Alternatively, condensation of (high-temperature) steam into the reservoir could also produce the observed dilution trend. To demonstrate this effect, we have selected the Cl-enriched fluid from well 24 of the East Bank to represent a typical, centrally located and high-temperature reservoir fluid (Fig. 6b). To this fluid we have added increasing mass fractions of equilibrium steam, at temperatures ranging from 230°C to 320°C. The resulting compositional envelope shows reasonable agreement with the other East-Bank discharges, with the exception of that from well 42 which is relatively enriched in ^{18}O. Most of the West-Bank fluids plot below the envelope, at slightly lighter $\delta^{18}O$ signatures. Whereas they could be argued to have a meteoric water component, it is clear that the same topology would apply to these discharges if the curves are shifted to slightly higher Cl contents.

The correlation between $\delta^{2}H$ and Cl (Fig. 6b) is considerably more complex than that described for ^{18}O and Cl. There are opposing trends for the two production fields, with the East Bank showing an inverse correlation between these constituents, and the West Bank showing a normal correlation. The data are compared once again to

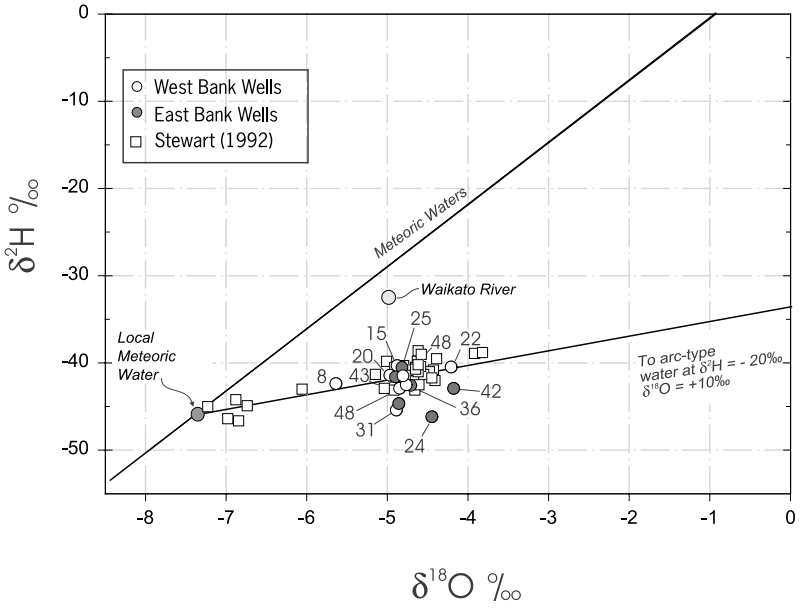

Fig. 5. $\delta^{18}O$–$\delta^{2}H$ isotopic signatures of the Ohaaki reservoir fluids. The discharge compositions are compared to local groundwater and Waikato River water.

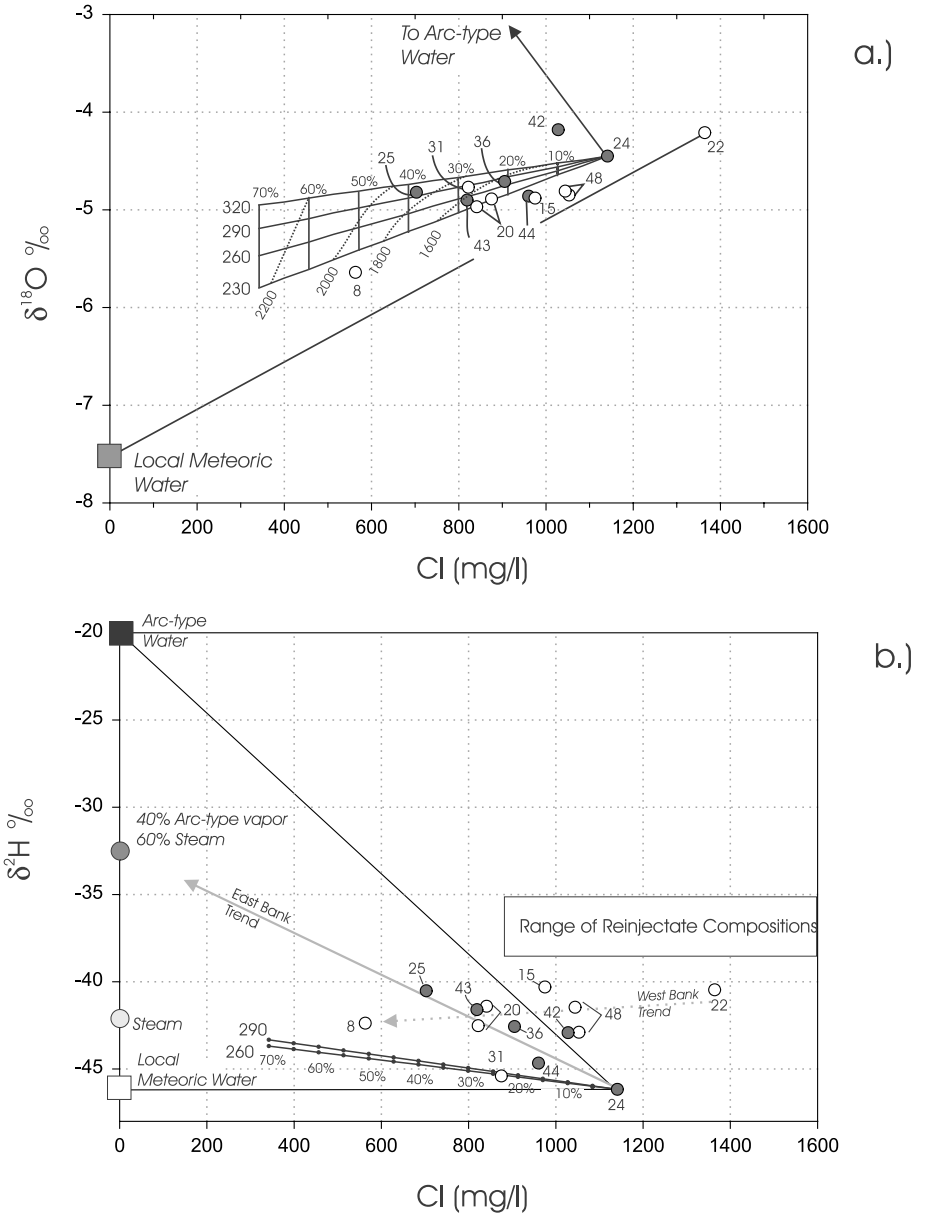

Fig. 6. (a) δ^2H–Cl and (b) δ^{18}O–Cl plots for the Ohaaki production fluids, compared to isothermal vapour gain/loss curves calculated for 270°C.

local groundwater, ATW, and to condensation pathways (as described above) for 260°C and 290°C) for well 24. For clarity, the 230°C and 320°C curves have been deleted from the figure, as they plot below the other pathways at lighter signatures that have little bearing on the discharge compositions. Noting that δ^2H signatures do not shift significantly with water–rock interactions (e.g. Giggenbach, 1992), the δ^2H signatures of the fluids depend only on mixing relationships between source components and physical reservoir processes such as boiling/condensation.

The West-Bank fluids trend toward an end-member diluent composition which lies close to

the δ^2H signature for bulk (geothermal) steam. The East-Bank fluids, on the other hand, trend from well 24 toward a Cl-free, δ^2H-enriched fluid of ca. 32‰, implying a significant component of ATW in the East-Bank reservoir. As discussed below, the two end-member components in the East-Bank reservoir water consist of a diluent with ca. 60% steam derived from meteoric fluid, 40% ATW, and an outflowing Cl-bearing fluid similar to that from well 24.

Whereas reinjection of separated waters has been under way since the field began production in 1989, the effects of reinjection returns on the distribution of ^2H and ^{18}O in the reservoir appear, at the present time, to be minimal or non-existent. Comparison of current signatures to those taken in 1990 (Stewart, 1992) and 1985 (Hedenquist and Stewart, 1985) indicates that the observed trends are independent of reinjectate component mixing (Fig. 6).

3.2.3. Equilibrium geoindicators

The alkaline-chloride nature of the reservoir fluids allows application of equilibrium thermodynamics as another means of assessing fluid processes in the reservoir. The discharge data are compared to the K–Mg and K–Na geoindicators of Giggenbach (1991), which are presented in orthogonal form (Fig. 7). The alteration assemblages (i.e. K-feldspar+illite+chlorite+quartz and K-feldspar+albite) on which these thermodynamic relations are based, are typically observed in the reservoir (Simmons and Browne, 2000; Hedenquist, 1990). Not surprisingly, the discharge data cluster around the full equilibrium line at temperatures ranging from 250°C to ca. 300°C, and correspond more or less to the measured reservoir temperatures. The discrepancy between the K–Mg and K–Na values for some discharges (e.g. 10 and 48) are likely to be the result of draw-down of minor amounts of steam-heated fluids into the production zone. These aggressive fluids are demonstrably enriched in Mg (cf. fluid from well 8, Table 1), and so plot closer to the immature boundary in Fig. 7.

3.2.4. Light and volatile element signatures in discharge waters

Apart from variations in water isotopes, so far there has been little to distinguish the West-Bank fluids or processes from their East-Bank counterparts. However, the distribution of more volatile solute species presents a rather different picture. It has long been recognised that there is a significant enrichment in B in the East-Bank production fluids (Fig. 8), where the maximum contents occur in

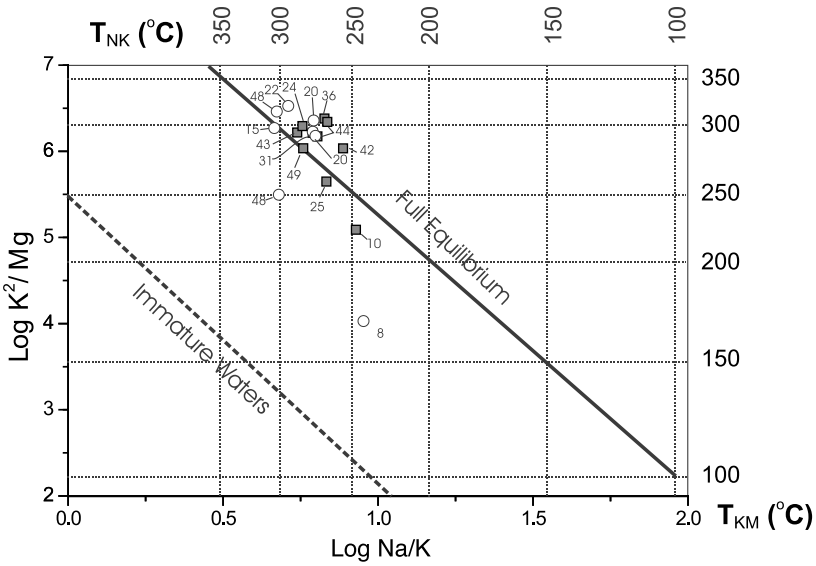

Fig. 7. Orthogonal plot of K–Mg and K–Na equilibrium temperatures of Giggenbach (1991).

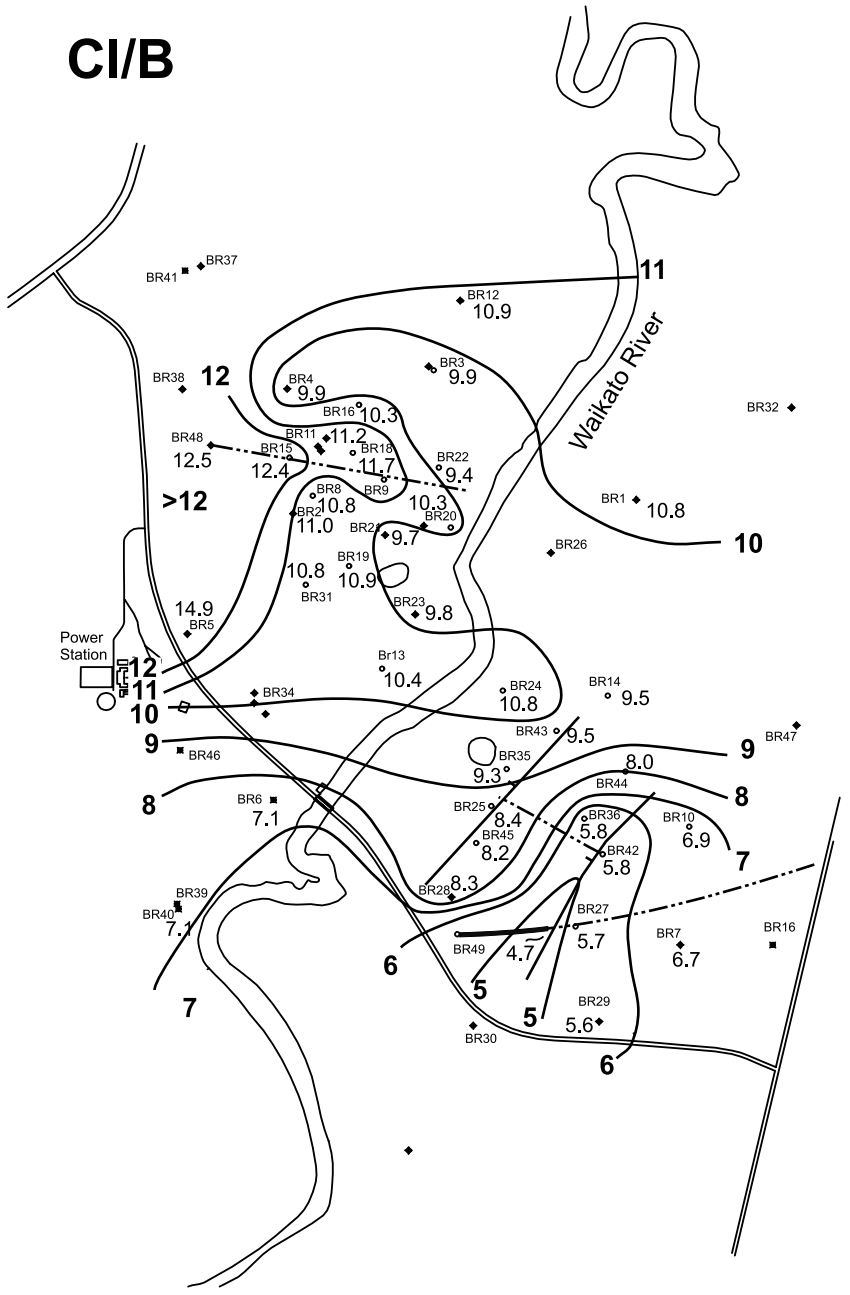

Fig. 8. Contoured Cl/B ratios across the Ohaaki field. So as to preclude exploitation effects influencing the topology, values plotted here are largely those from Hedenquist (1990), with data for newer (i.e. deeper) wells from Contact Energy (well 49) and this study. Cl/B minima occur in the SE corner of the field.

the vicinity of wells 49 and 42, and the values monotonically decrease to the north and west of the system.

The enrichment in B relative to Cl on the East Bank was first reported by Mahon and Finlayson (1977), who considered the anomaly to be the result of the closer proximity of greywacke basement rocks here to production zones (cf. Fig. 3).

This explanation was taken up by Hedenquist (1990) who suggested that B was rapidly fixed in hydrothermal minerals forming in the volcanic units as fluids discharged into them from the underlying, B-enriched greywackes. Giggenbach (1989), however, recognised that Cl/B ratios generally decrease across the TVZ towards the east, and suggested that the East-Bank B anomaly may result from the direct input of B here from a young andesitic intrusion.

If the proximity of greywacke to the production horizons was responsible for the observed variations in fluid Cl/B ratios at Ohaaki, one would expect a vertical stratification of Cl/B water values, or at least a similar zonation in other systems that have large basement offsets. In fact, there is a subtle correlation between Cl/B and feed-zone depth in production wells at Ohaaki (e.g. Glover and Hedenquist, 1989), but the effect is minimal in comparison to the spatial Cl/B variation, and the values are complicated by cross-flows in the system. By comparison, the Kawerau system, which has more than 800 m offset of the basement across the drilled portions of the field, has near-uniform Cl/B ratios (Christenson, 1997).

The issue as to whether the greywacke is indeed higher in B relative to the overlying volcanic lithologies also deserves further examination. The early hydrothermal experiments of Ellis and Sewell (1963) showed that dissolution of TVZ greywacke did indeed generate waters with low Cl/B ratios, which is consistent with their being a source rock of B in the TVZ. However, the results of their individual experimental runs show that, in absolute terms, the amount of B released from the greywacke varied over the same range as the other (volcanic) lithologies tested. In fact, proportionally more B was released from the volcanic rocks than from greywacke. Given that both elements were readily leached from the greywackes, the explanation for low Cl/B ratios in the reacted waters was that the greywackes are relatively deficient in Cl. Furthermore, the inherently impermeable nature of the greywacke suggests that permeability within the basement rocks is fracture-related, and as pointed out by Reyes and Vickridge (1996) adjacent to these fractures would have been rapidly 'flushed' from the system. So, even though the greywacke is a possible source of B, the proximity arguments made previously are probably not valid, especially in light of the suggestion that alteration on the East Bank is older than that on the West (Hedenquist, 1990).

Relative Li–B–Cl contents for the discharges are compared to three common TVZ lithologies and to volcanic crater lake compositions in Fig. 9. Apart from wells 25 and 10, the East-Bank discharges are clearly enriched in B relative to their West-Bank counterparts. Wells 25 and 10, with signatures similar to the most Li-enriched discharges on the West Bank, have recently produced increasingly dilute, HCO_3^--rich waters indicating draw-down of shallow, steam-heated fluids into the production zone. As mentioned above for well 8, these aggressive fluids carry cation signatures closer to their host reservoir rock composition (i.e. rhyolite) than the deeper, less aggressive waters.

Even so, all discharges are Li-depleted relative to the potential source rocks, which is consistent with this element entering into hydrothermal alteration phases (Reyes and Vickridge, 1996). Although there is some overlap of compositional ranges, it is of interest to note that the East-Bank discharges appear to have closer similarity to the Cl/B values of the White Island andesite, whereas the West-Bank compositions are more similar to the average TVZ rhyolite. Crater lake waters from Ruapehu and White Island, which are representative of magmatic–hydrothermal fluids, are strongly enriched in Cl relative to either the Ohaaki fluids or any of the TVZ lithologies, suggesting that magmatic volatiles alone cannot account for the observed reservoir compositions.

Owing to our ignorance of the deep reservoir environments, the ultimate source(s) of B and Cl in the Ohaaki fluids remains somewhat equivocal. Although the TVZ volcanic lithologies have Cl/B values similar to those of the Ohaaki discharges, the volcanic units occur only in the upper 1–2 km of the reservoir (Fig. 3) and hence are unlikely to contribute significantly to the source fluid compositions. As discussed by Ellis and Mahon (1964) and shown in Fig. 9, the greywacke basement rocks are a possible source of B, but the fluids moving through them are relatively depleted in

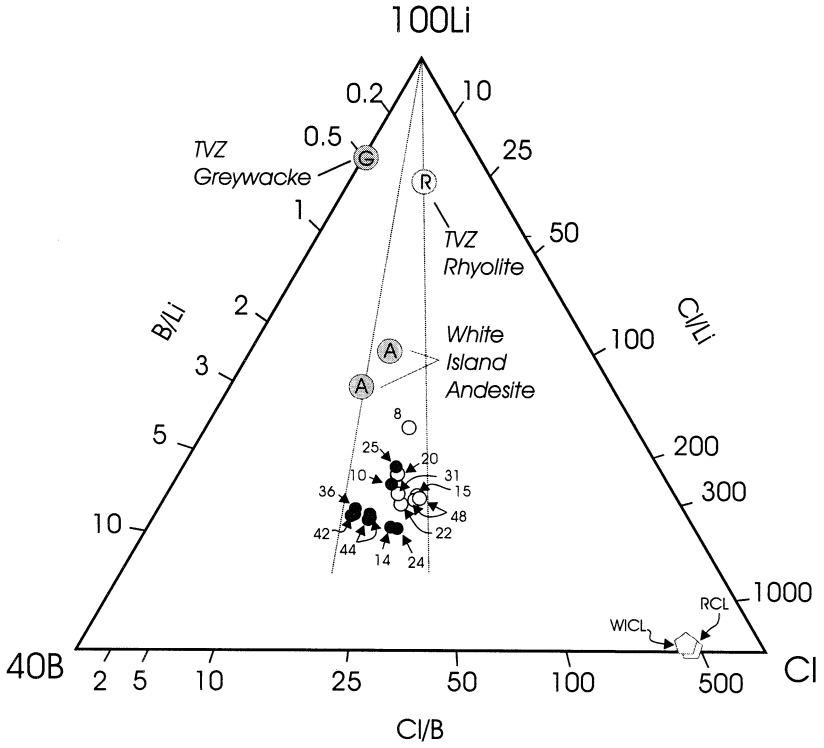

Fig. 9. Relative contents of Li–B–Cl in the Ohaaki reservoir fluids. Discharge data are compared to typical White Island andesite (Wardell et al., 2000), average rhyolite and average TVZ greywacke (Reyes and Vickridge, 1996), White Island crater lake (WICL, Christenson, unpublished data) and Ruapehu crater lake (RCL, Christenson, 2000).

Cl. It is not known what lithologies underlie the greywacke in the TVZ, but perhaps intrusions at depth provide the appropriate Cl/B signatures.

Direct magmatic volatile inputs must also be considered as potential sources for both Cl and B in the Ohaaki fluids. B is readily transported in high-temperature vapours as H_3BO_3 (Quisefit et al., 1989), but with decreasing temperature under subcritical conditions, B partitions increasingly into the higher-density phase (Glover, 1988). Since crater lakes serve as fairly efficient condensers of high-temperature magmatic gas (Giggenbach, 1974), and noting that there are no B minerals stable in the lake waters (Christenson and Wood, 1993), it seems reasonable to expect that B behaves conservatively in these systems. Cl is of course also readily transported in high-temperature magmatic gas streams as $HCl_{(g)}$, but under subcritical conditions, its volatility becomes a function of pH and Cl concentration of the high-density phase. With steady-state conditions of heat- and mass-flow into the crater lakes, the Cl values of these typically low-pH, high-salinity waters should be considered as minimum values (allowing for minor losses of HCl gas to the atmosphere). This suggests then that the Cl-enriched Cl/B ratios for crater lake waters plotted in Fig. 9 are also minimum values, leading then to two possible explanations for the low Cl/B ratios in the East-Bank fluids at Ohaaki. Either they reflect dissolution of a volcanic-intrusive lithology within the basement greywacke complex, or the dissolution of B-enriched greywacke basement rocks by aggressive HCl-bearing magmatic fluids.

Relative contents of F, Cl, and B in the Ohaaki discharges are portrayed in Fig. 10, where most East-Bank discharges are shown to be significantly enriched in F compared to the West

Table 3
Composition of steam discharged from Ohaaki production wells

Well	CT (°C)	He	H_2	O_2	N_2	CH_4	Ar	H_2S	CO_2	NH_3	CO	X_g (μm/m)	H_2O	$\delta^{18}O_{stm}$ (‰)	$\delta^{2}H_{stm}$ (‰)	$\delta^{13}C_{CO_2}$ (‰)	$\delta^{13}C_{CH_4}$ (‰)	R/R_A	$^{40}Ar/^{36}Ar$	$T_{\Delta Md}$ (°C)	T_{HA} (°C)
Production well discharges																					
BR8	149	0.24	287.8	< 0.05	1 339	2 427	2.58	463	56 157	234.8	0.10	6 0912	939 088	−8.64	−56.5	−8.4	−26.5	5.59	298.6	410	318
BR15	210	0.03	21.0	0.05	110	201	0.29	125	7 605	347.1	0.48	8 410	991 590	−6.45	−43.7	−8.3	−26.3	4.80	299.6	412	305
BR20	177	0.02	17.3	< 0.05	113	224	0.38	123	9 884	277.0	na	10 638	989 362	−7.12	−44.8	−8.0	−26.5	na	na	395	291
BR22	183	0.03	38.0	0.20	155	304	0.41	200	13 822	275.9	na	14796	985 204	−6.15	−44.5	−8.7	−26.7	4.40	297.8	412	312
BR24	170	0.04	53.8	< 0.05	127	243	0.39	199	12 479	34.5	na	13137	986 863	−6.61	−49.7	−7.8	−26.5	na	na	396	325
BR25	188	0.02	5.9	0.29	50	102	0.22	73	8159	198.3	na	8 589	991 411	−6.69	−45.5	−9.5	−26.7	4.80	301.4	430	276
BR31	147	0.08	155.2	< 0.05	226	394	0.55	310	22 272	63.1	na	23 421	976 579	−7.41	−53.8	−8.1	−26.1	na	na	411	346
BR36	179	0.03	122.4	< 0.05	139	265	0.27	251	16 891	294.6	na	17 964	982 036	−6.52	−42.8	−8.0	−25.8	3.60	318.3	417	360
BR42	199	0.04	150.5	0.25	218	413	0.30	247	23 774	453.3	0.08	25 257	974 743	−5.93	−42.8	−8.9	−25.8	3.13	304.4	437	364
BR43	186	0.06	50.9	0.87	247	409	2.20	230	18 979	254.8	0.02	20 174	979 826	−6.65	−45.1	−8.8	−26.2	5.54	298.4	425	270
BR44	179	0.04	132.4	< 0.05	194	340	0.45	296	20 100	381.6	na	21 443	978 557	−6.59	−45.0	−7.5	−26.4	3.63	318.0	415	348
BR48	163	0.08	62.9	< 0.05	271	504	0.76	308	18 609	313.6	na	20 069	979 931	−6.82	−48.5	na	na	na	na	na	309
BR49	186	0.08	134.0	< 0.05	369	651	0.50	297	32 635	366.9	na	34 454	965 546	−6.09	−44.2	−8.4	−26.0	2.58	305.5	420	345
Bleed-line gas samples																					
BR26		3.73	4 980.0	< 0.05	17 440	32 042	34.36	6471	939 030	na	na	1 000 000	0	na	na	−6.4	−26.2	na	na	376	326
BR17		2.14	2 594.2	< 0.05	12 339	21 194	27.05	4 386	541 050	131.2	na	581 725	418 275	na	na	−7.1	na	na	na	na	314
BR5		6.50	48.7	36.06	39 073	65 846	64.11	2 984	690 096	na	na	798 153	201 847	na	na	−6.3	−26.6	4.59	301.9	366	167
BR1		3.39	2677.9	< 0.05	15 594	29 085	25.01	3 003	914 680	9.7	na	965 078	34922	na	na	−6.1	−27.6	na	na	345	317
BR9		0.49	5 473.3	< 0.05	6 349	13 069	18.61	9 218	812 293	3.1	na	846 425	153 575	na	na	−7.1	−26.3	na	na	386	348
BR10		2.78	2 292.5	< 0.05	13833	23 293	29.92	3 224	693 530	6.7	na	736 212	263 788	na	na	−7.0	−25.4	2.95	321.9	404	307
BR33		0.02	228.0	1.71	131	349	0.57	617	55 528	39.9	na	56 895	943 105	na	na	−8.9	−27.7	na	na	395	357
BR14		0.05	243.5	< 0.05	263	450	0.74	386	21 315	66.2	na	22 725	977 275	na	na	−7.7	−26.2	na	na	401	351
BR7		6.26	2 816.6	0.00	35 140	54 312	68.26	3 554	795 146	na	na	891 043	108 957	na	na	na	na	2.81	314.6	na	288

All concentrations as μmol/mol. T_{MC}, ^{13}C CH_4–CO_2 fractionation temperature; T_{HA}, H_2–Ar geothermometer temperature.

Bank. Saturation calculations show that F contents are not solubility-controlled by fluorite in any of the discharges.

The discharges are compared to temperature-indexed B–Cl–F data from a fumarolic discharge on White Island volcano, to compositions of Ruapehu crater lake water (Christenson, 2000), to TVZ rock compositions (Ellis and Mahon, 1964), and to a larger data set of temperature-indexed Cl/F ratios from White Island (Giggenbach and Sheppard, 1989). Collectively, the fumarolic data suggest that relative fluoride contents of the discharges vary directly with temperature in these environments. The position of Ruapehu crater lake water indicates the discharge of a high-temperature magmatic gas stream into the vent hydrothermal system, which is consistent with the findings of Christenson and Wood (1993). In this context, the high F values in the East-Bank discharges may result from the condensation of magmatic volatiles at temperatures approaching 400°C, whereas the West-Bank fluids derive from a cooler, or F-depleted source. Alternatively, the enrichment in F in the East Bank could be explained by the local (enhanced) dissolution of F-bearing reservoir rocks. As described above, this scenario requires increased hydrolysis capability which, of course, is consistent with elevated magmatic volatile contents.

4. Chemical and isotopic characteristics of gas discharges

4.1. Chemistry of non-condensable gases

Chemical and isotopic data for gases discharged from the Ohaaki wells are listed in Table 3. In general, the gas compositions are similar to those discharged from other geothermal fields in the TVZ, with the redox state of the fluids being controlled by the $FeO–FeO_{1.5}$ rock buffer. What sets the Ohaaki fluids apart from most other TVZ systems is the high total discharge concentration of gas in the discharges, with non-condensable gas contents ranging up to 1 mol (ca. 4% b.wt.). The high gas yields led

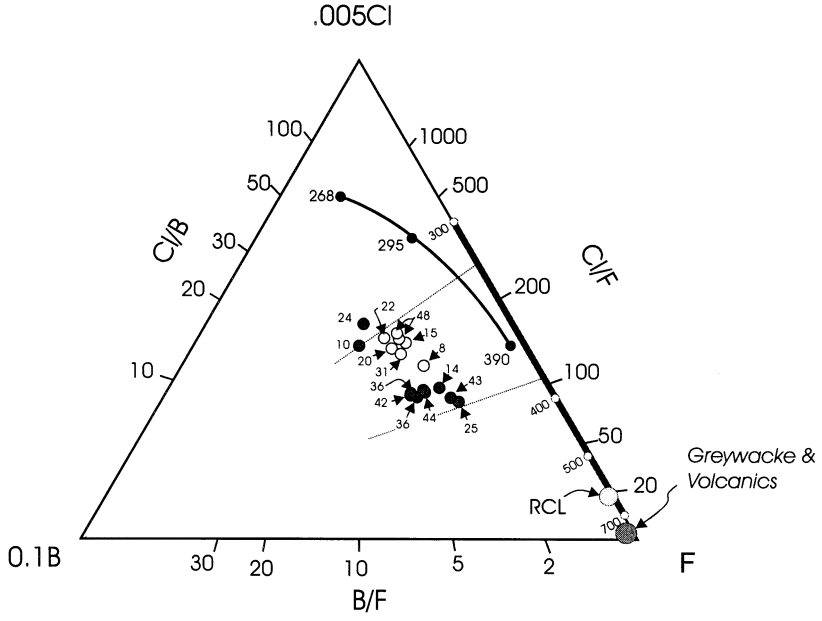

Fig. 10. Relative contents of Cl–B–F. Data are compared to temperature-indexed compositional Cl–B–F trends from White Island, temperature-indexed Cl/F ratios from White Island (Giggenbach and Sheppard, 1989; Christenson, unpublished data), and to Ruapehu crater lake compositions (Christenson, 2000).

Grant (1977) to regard the system as 'gas-dominated', with natural two-phase conditions extending to at least 2 km depth. Owing to the two-phase nature of the system, rigorous calculation of the CO_2 content of a possible single-phase source fluid is impossible.

Thermodynamic assessment of the gases is likewise complicated by the high enthalpies of many of the discharges (Table 2). This is demonstrated through comparison of the total discharge CH_4 and CO_2 compositions at the reservoir temperatures (defined by the quartz equilibrium temperature, T_{qz}, Table 2) to the temperature-dependent equilibrium ratios for these gases (Fig. 11, adapted from Giggenbach, 1980). Most of the discharges plot in the 'vapour gain' field confirming that the discharges represent non-equilibrium mixtures of vapour and liquid. Nevertheless, valuable information regarding source fluid characteristics can still be obtained.

As pointed out by Giggenbach (1989, 1995), the non-reactive gases (e.g. N_2–Ar–He) discharged from wells at Ohaaki have many characteristics in common with those discharged from arc-type volcanoes (Fig. 12). Here the gases are compared to the range of compositions observed in arc-type discharges, air, air-saturated water and to crustal gases which are normally enriched in radiogenic He. The Ohaaki discharges plot along a line connecting N_2-rich arc-type gases with air components. There is little to distinguish the East- and West-Bank fluids, both of which have amongst the highest N_2/Ar ratios in the TVZ, suggesting that the heat source(s) in both production fields have similar arc-type affinities.

If we accept that the majority of Ar in these systems is of atmospheric origin (Giggenbach, 1991), then the N_2/Ar ratio can be used to identify their source upwelling(s) within the system (Fig. 13). The highest N_2/Ar values are found in the southern part of the field on the East Bank (wells 42 and 49), and these are linked via a broad zone of elevated N_2/Ar ratios to another local East Bank high in the vicinity of BR1. Another, less extensive area of elevated N_2/Ar ratios is found on the West Bank, and appears to delineate the basement fault shown in Fig. 3. The maximum ratio of 609 from well 5 is of interest in

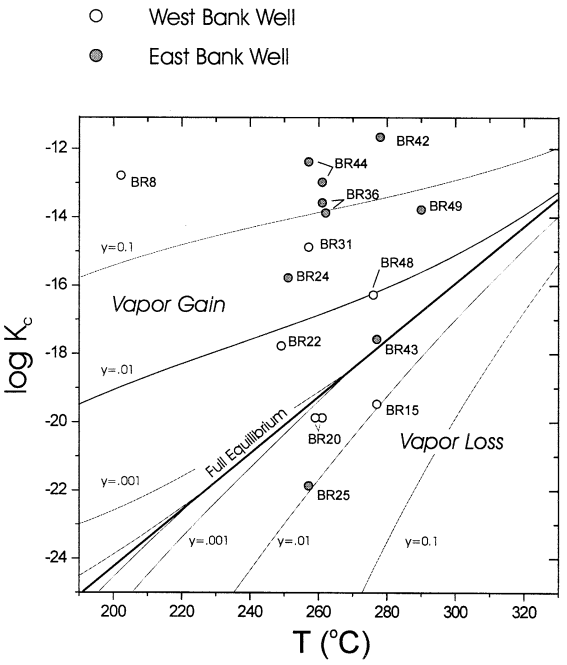

Fig. 11. Log K_c for West- and East-Bank discharges at their respective quartz equilibrium temperatures compared to log K vs. T for the Fischer–Tropsch reaction, and isopleths for steam fractions added/lost from the fluid. Modified from Giggenbach (1980).

that it is situated at the field margin as defined by the resistivity boundary at 1000 m depth (Fig. 2).

The maximum ratio in the field is 747 from well 42. Along with fluids from well 49, this well also yields the minimum measured Cl/B ratios, clearly identifying a major source upwelling for the field. It appears that fluids here rise along another of the inferred basement faults, in this case, the one forming the western side of a basement horst block (Fig. 3). The local high N_2/Ar ratio in the vicinity of well 1 may also relate to some fault structure, possibly en echelon to the NE-trending structure to the south, but this needs to be proven from further drilling.

A comparison of the relative total discharge He–CO_2–Cl contents of the fluids (Fig. 14) shows the East-Bank wells to be enriched in CO_2 relative to those on the West Bank. As a check to see if the eastern discharge compositions can be derived from those to the west through boiling, a single-

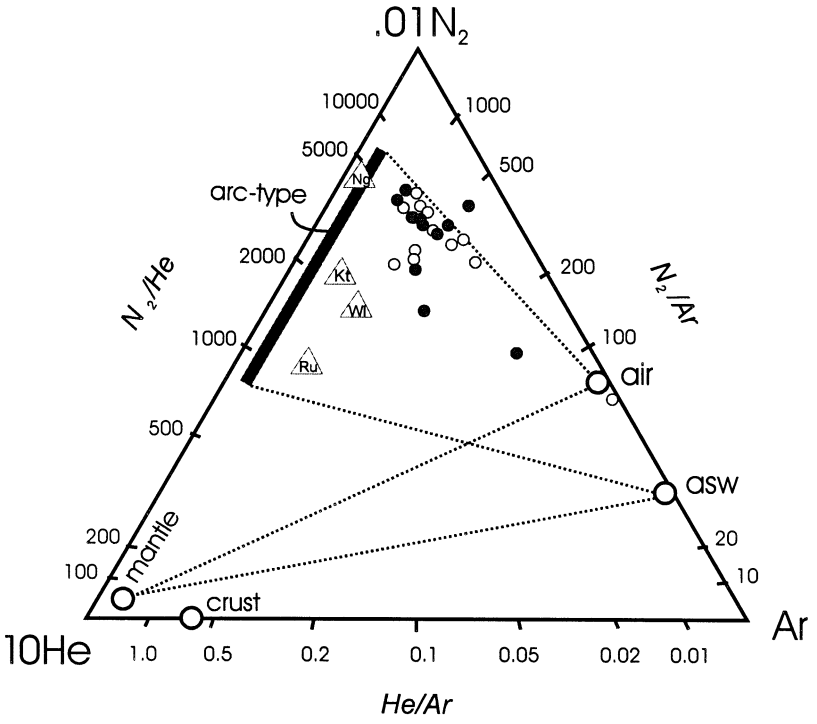

Fig. 12. Relative contents of N_2–He–Ar for East- and West-Bank discharges, compared to arc-type, mantle, crustal, air and air-saturated water gas compositions, and to a range of New Zealand volcanic arc discharge gases (Ru, Ruapehu; Kt, Ketatahi; Ng, Ngauruhoe; and WI, White Island). Adapted from Giggenbach (1995).

stage isenthalpic cooling pathway has been constructed for the fluid of well 48. This fluid was chosen because it has the highest relative gas contents from the West Bank, with little evidence of steam heating. The results show that the liquid-phase envelope encompasses all of the other West-Bank fluid compositions except that for well 8, which shows evidence for mixing between the parent fluid and vapour derived from a 20% mass fraction separation. The latter is consistent with both the Cl–enthalpy characteristics and the relative CH_4–CO_2 contents of the discharge (Figs. 4 and 11 above).

The discharge data in Fig. 14 are also compared to time series data for some 26 fumarolic discharges from White Island fumarole #3 (Giggenbach and Sheppard, 1989; Christenson, unpublished data), collected over a temperature range of 100–772°C. The relative CO_2 contents from White Island correspond closely to the range of compositions exhibited by the CO_2-enriched East-Bank fluids, with CO_2/He ratios ranging between 300 000 and 700 000. This suggests that the fluids discharged on the East Bank are less evolved (i.e. have interacted less with the reservoir rocks) than those on the West Bank.

Not surprisingly, there is a negative correlation between CO_2 and Cl/B in the discharges (Fig. 15), pointing to a common source for CO_2 and B on the East Bank. The implications of this correlation are discussed below.

4.2. ^{13}C signatures of discharge gases

$\delta^{13}C_{CO_2}$ values for the deep discharges range from −7.5‰ to −9.5‰ (Table 3; Fig. 16). There is little observable distinction between the East- and West-Bank compositions, and collectively the deep fluids have a mean $\delta^{13}C_{CO_2}$ value of −8.3‰, and a standard deviation of 0.5‰. Bleed-line samples show a wider compositional range for $\delta^{13}CO_2$ (−6.4 to −8.9‰), possibly re-

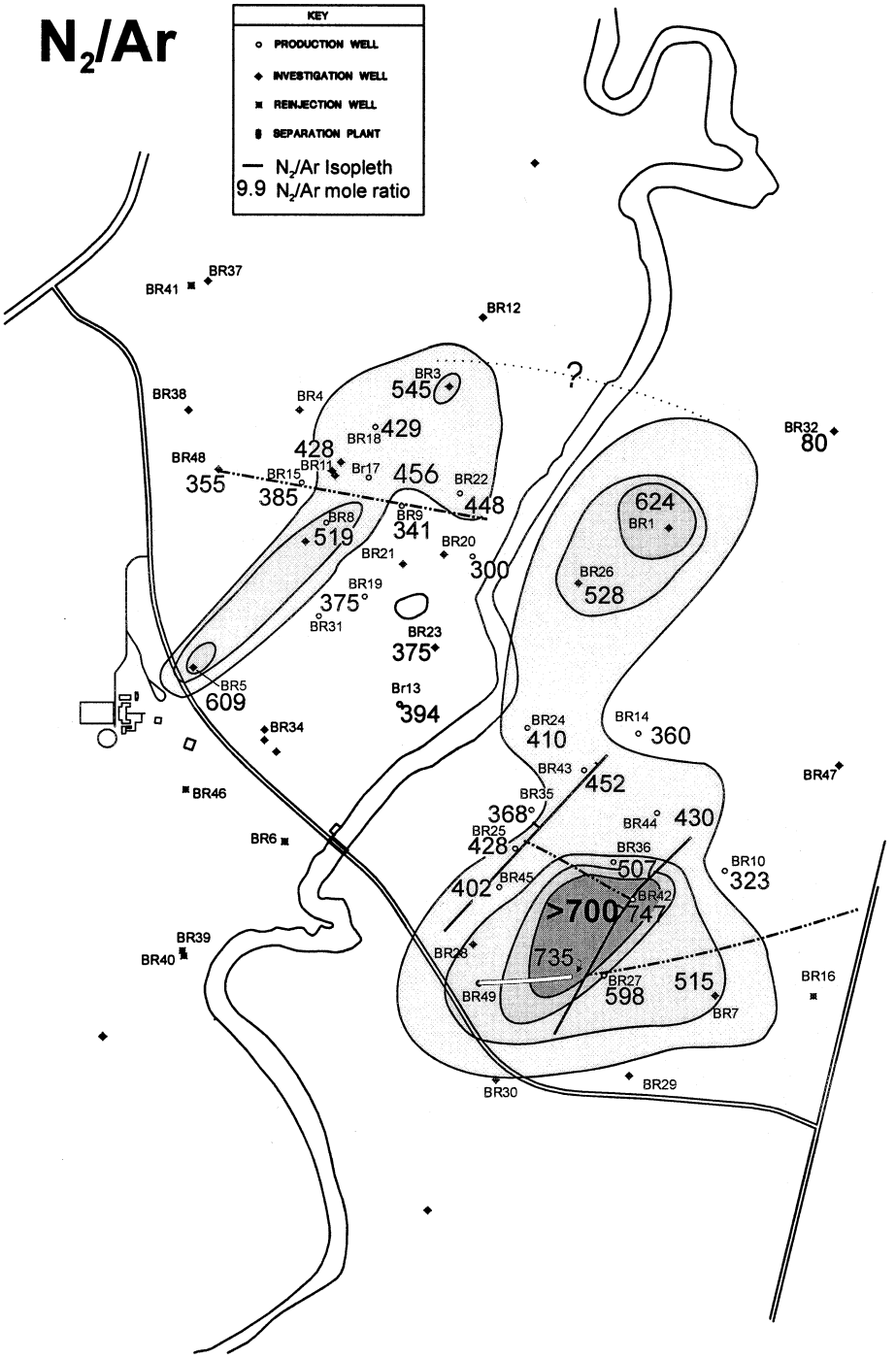

Fig. 13. N_2/Ar ratios across the Ohaaki field.

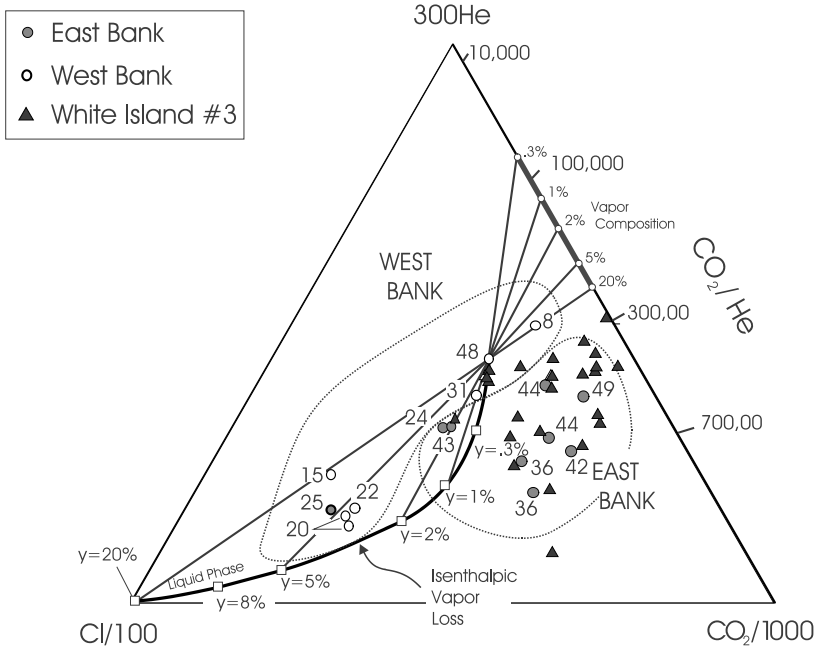

Fig. 14. Relative contents of He–Cl–CO_2 in fluid discharges for the Ohaaki field, compared to a single-stage isenthalpic cooling pathway calculated for the discharge from well 48 showing liquid- and vapour-phase compositions (squares and circles, respectively).

flecting boiling-induced fractionation and/or associated calcite deposition in the respective wellbores. The deep fluids have $\delta^{13}C_{CO_2}$ signatures coinciding with the isotopically lighter end of the range of typical mantle values (-6.5 ± 2.5; e.g. Nishio et al., 1998), and data positions in Fig. 16 are consistent with a predominantly magmatic origin for the carbon, with perhaps a small contribution from organic (i.e. kerogen) sources. The $\delta^{13}C_{CH_4}$ values range between -25.8 and -26.7 in the deep fluids, and have a mean value of -26.4 and a standard deviation of 0.3.

The $\delta^{13}C$ signatures of CO_2 and CH_4, and their equilibrium fractionation temperatures in the discharges (Table 3) are summarised in Fig. 16 where the data are compared to equilibrium fractionation isotherms and two possible end-member C source components. The $^{13}CH_4$–$^{13}CO_2$ isotope equilibration temperatures have an advantage over their chemical equilibrium counterparts in that they are not sensitive to excess enthalpy conditions, and hence more accurately reflect conditions in the reservoir at the point and time of equilibration. On the other hand, isotope exchange kinetics are significantly slower than their chemical counterparts (e.g. Giggenbach, 1997), and as such are therefore more likely to preserve deeper equilibrium temperatures.

From Table 3 and Fig. 16, the equilibrium temperatures span a range of 366–437°C across the

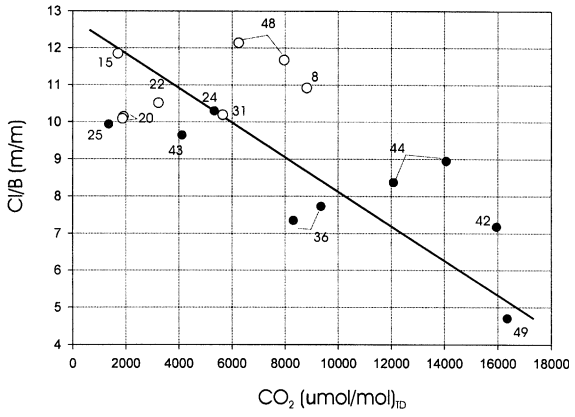

Fig. 15. Ohaaki reservoir Cl/B plotted as a function of total discharge CO_2 contents.

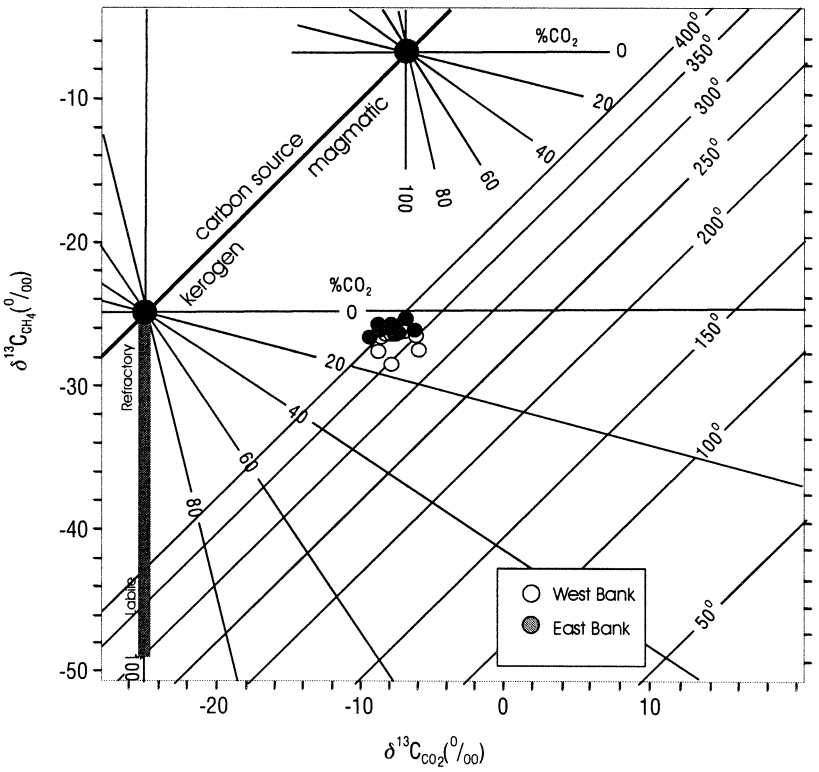

Fig. 16. CH_4–CO_2 ^{13}C compositions for East- and West-Bank production discharges. Data are compared to equilibrium fractionation isotherms and possible end-member carbon sources. Modified from Giggenbach (1997).

field. Temperatures associated with the main N_2/Ar anomaly on the East Bank are uniformly above 400°C, with a maximum of 437°C for the gases from well 42. Equilibrium fractionation temperatures for the West-Bank discharges are generally lower, ranging from 345°C to 412°C. The two outlying N_2/Ar ratio maxima for wells 5 and 1 (Fig. 13) have equilibration temperatures considerably lower than measured in the central plumes, pointing perhaps to the complex relationship which exists between flow velocity, depth and reaction kinetics in the reservoir.

4.3. Noble gas isotope characteristics

$^3He/^4He$ and $^{40}Ar/^{36}Ar$ data for the production fluids available between 1978 and 1986 were published by Hulston and Lupton (1996). They reported that $^3He/^4He$ values from the West Bank were significantly higher than those from the East Bank, and the East-Bank fluids had considerably more radiogenic $^{40}Ar/^{36}Ar$ ratios. They suggested that this difference was due to leaching of ^4He from the basement greywackes, but did not explain why this should be observed on the East Bank and not on the West Bank. In the present work, we sought to add to the existing data set for the Ohaaki field, particularly with respect to gases from newer production wells on the East Bank so that all results could be collectively assessed.

$^3He/^4He$ and $^{40}Ar/^{36}Ar$ data obtained for this study are listed in Table 3, and are plotted along with that of Hulston and Lupton (1996) in Fig. 17. There is reasonable agreement between the earlier $^3He/^4He$ data and the results presented here, but the $^{40}Ar/^{36}Ar$ values from the current study are notably higher. The reason(s) for this discrepancy is unknown, but may reflect on changes in the reservoir brought about by 10 years of production from the field. Nevertheless, there is broad agree-

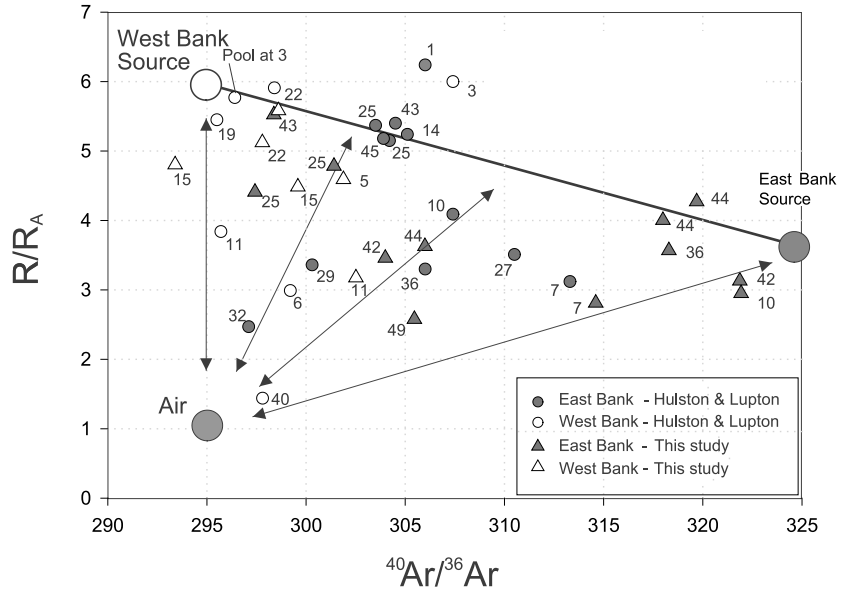

Fig. 17. R/R_A vs. $^{40}Ar/^{36}Ar$ for Ohaaki production fluids, including data from Hulston and Lupton (1996) and this study.

ment between the two studies with respect to an overall trend of increasing radiogenic components (^4He and ^{40}Ar) from west to east. The distribution of data can be explained in terms of three-component mixing between a rather MORB-like West-Bank source gas with $R/R_A \approx 6.0$ and $^{40}Ar/^{36}Ar$ of 295, an East-Bank source gas with $R/R_A \approx 3.5$ and $^{40}Ar/^{36}Ar$ of 324, and air ($R/R_A \approx 1.0$ and $^{40}Ar/^{36}Ar$ of 295).

It is noteworthy that with the exception of well 49, the East-Bank discharges positioned closest to the inferred radiogenic-enriched end-member composition in Fig. 17 are from wells lying closest to the basement fault structure which coincides with the highest N_2/Ar and lowest Cl/B ratios in the field. Rare gas signatures from well 49 show evidence of air contamination; projection of the well 49 composition back to the east–west mixing line, however, shows that it too is relatively enriched in radiogenic gases. Again, this area corresponds to the main fluid upwelling on the East Bank, and is therefore a highly desirable target for future deep drilling in the field.

The relationship between CO_2 and ^3He to R/R_A in the reservoir fluids is shown in Fig. 18a where the Ohaaki discharges are compared to end-member MORB mantle compositions and crustal fluids of different $CO_2/^3He$ ratios. Collectively the fluids plot at $CO_2/^3He$ values considerably higher than those of MORB (Marty and Jambon, 1987), consistent with the views of both Hulston and Lupton (1996) and Giggenbach (1995) that the fluids include a significant C contribution from crustal sources. The East-Bank fluids have higher $CO_2/^3He$ ratios than those from the West Bank, and the negative correlation between R/R_A and $CO_2/^3He$ is consistent with MORB-type gas mixing with a crustal end-member component having a maximum $CO_2/^3He$ of ca. 2.5×10^{11}. These values, which are similar to those observed in sedimentary basins, are higher than the values reported in Hulston and Lupton (1996).

Further insight into the origins of the crustal carbon component is provided through application of the treatment developed by Sano and Marty (1995) which correlates ^{13}C with $^3He/^4He$. Three end-members are considered in their formulation, including MORB gases, marine limestone and organic carbon-rich marine sediment, which, respectively, represent the three vertices of Fig. 18b. The results show that the C from both production fields is dominated by a limestone car-

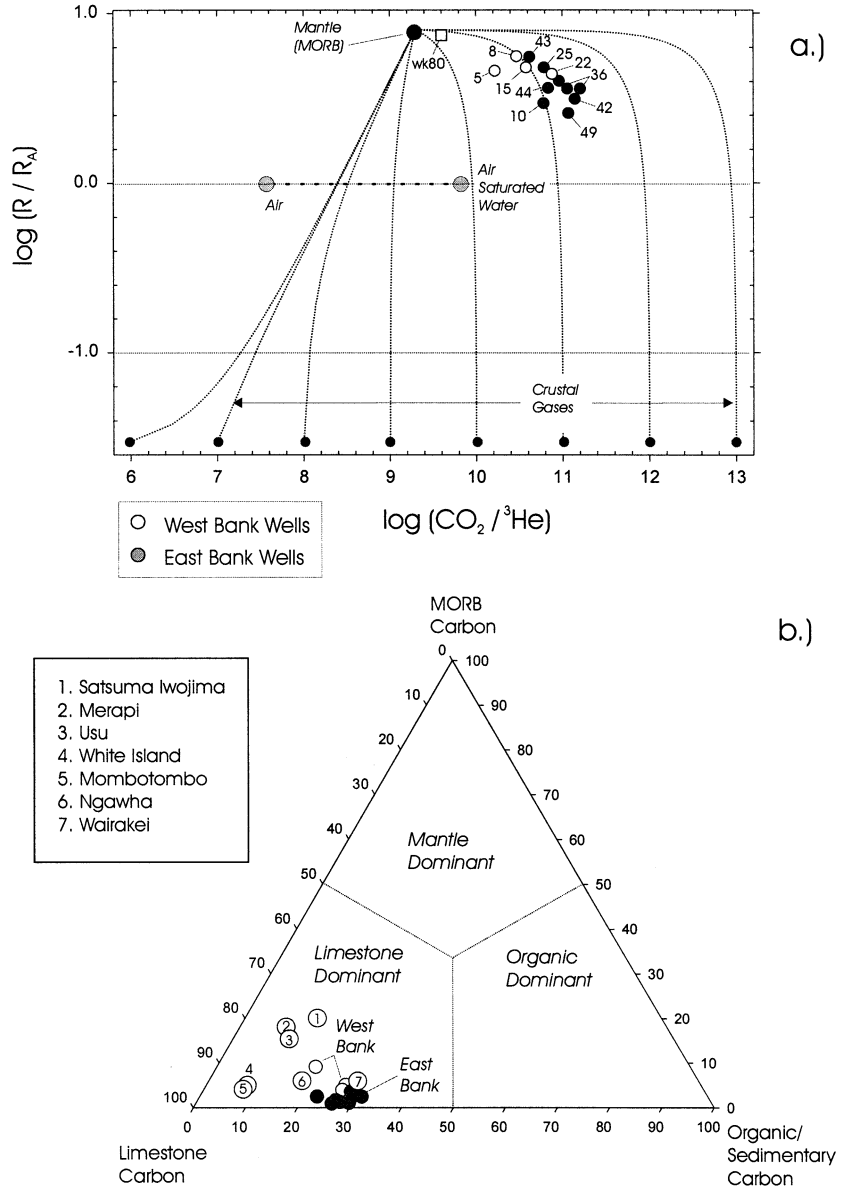

Fig. 18. (a) R/R_A vs. $CO_2/^3He$ plotted against contours for various crustal gas compositions. East- and West-Bank discharges are compared to signatures for air, air-saturated water, MORB mantle gas, and to a range of crustal gas end-member component compositions with $CO_2/^3He$ ratios ranging from 10^6 to 10^{13}. The Ohaaki discharges are mixtures between a MORB-type mantle gas and a crustal gas with a $CO_2/^3He$ ratio of ca. $10^{11.5}$. Although plotting at lower observed $CO_2/^3He$ ratio, a single sample from the Wairakei production field (wk80) not surprisingly has similar end-member components to those at Ohaaki. (b) Carbon source contributions to the Ohaaki discharges, plotted in terms of three end-member components (marine limestone, marine sediments and MORB-type mantle gas).

bon source (ca. 70%), and that the East-Bank fluids are slightly enriched in this end-member over those from the West Bank. The results also indicate a comparatively small mantle C component in the discharges, with perhaps slight relative enrichment in this end-member in the West-Bank discharges.

Unfortunately, this methodology does not al-

low discrimination between subducted carbonate-bearing sediments and contributions from assimilated crust (e.g. carbonate contained in greywacke basement rocks). Comparison of the Ohaaki discharges to those from high-temperature arc-type volcanoes, including White Island (Sano and Marty, 1995), and to the Wairakei and Ngawha geothermal systems in New Zealand shows that the geothermal system gases are relatively enriched in the limestone carbon over their higher-temperature counterparts. This suggests that the large, hot-water systems in New Zealand have a minor, but measurable contribution of carbonate C from the basement rocks.

5. Discussion and conclusions

5.1. Location of the heat sources

Collectively, the above results are consistent with the suggestion of Giggenbach (1989) that two distinctly different source fluids discharge into the Ohaaki reservoir. The differences between these fluids are most clearly expressed in their less reactive, volatile-constituent signatures, with the East-Bank fluids being volatile-enriched, and less evolved (i.e. more magmatic) than their western counterparts. The more reactive, non-volatile constituents (e.g. alkali and alkaline-earth metals) appear to more readily equilibrate with reservoir rocks at local conditions, masking information about the heat source environment.

Questions which remain unresolved for the Ohaaki system, and which are of utmost interest to the field operators, pertain to the depths and physico-chemical characteristics of the respective heat sources. Whereas observed differences in source fluid chemistry probably reflect the relative ages of the intrusives, with the East Bank being considerably younger (Giggenbach, 1989), the effects of dispersion of the upwelling source fluids must be considered. In our view, the short distances over which the geochemical anomalies between the East Banks and West Banks are observed suggests that the East-Bank heat source probably resides at a shallower depth than that on the West Bank. If degassing magma was as deep as 8 km, in accordance with the 'hot-plate modelling' referred to previously, the geochemical signatures observed in the respective production reservoirs would be expected to be far less distinct owing to diffusion and co-mingling of the fluids during their ascent.

Unfortunately, it is not possible to unequivocally quantify the depth to an intrusive body on the East Bank with the geochemical data to hand, and there is no geophysical information presently available with which to resolve the problem. We do know that the heat sources on both banks lie below the drilled reservoir, as there has been no indication of the alteration style or intensity encountered in the alteration halo as is associated with the Ngatamariki intrusive. At Ngatamariki the alteration halo extends ca. 1000 m above the intrusive contact (Christenson et al., 1998), which is similar to the dimensions of the so-called contact metamorphic zone occurring over the relatively shallow granitic intrusion intersected by drilling at Kakkonda, Japan (Doi et al., 1998).

We are, however, able to establish some constraints on the depth to the brittle–plastic transition (hereafter BPT) zone associated with the intrusive. One approach is to consider the boiling-point–depth relationship for the reservoir fluids, being mindful of the fact that the calculated minimum depth of first boiling increases coherently with gas (principally CO_2) contents. If the top of the BPT is at a temperature of ca. 370°C (e.g. Fournier, 1999), and if we accept that the upwelling fluid has a CO_2 content of ca. 4.4% by mass (i.e. 1 mol, Sutton and McNabb, 1977), then we can calculate a minimum depth of ca. 2700 m to the BPT zone, assuming saturated vapour conditions and cold (10°C) hydrostatic confining pressures. Using observed pressure/depth constraints from the Ohaaki field (unpublished data, Contact Energy), the calculated depth to the 370°C isotherm is ca. 3100 m.

An overriding assumption in these calculations is that the reservoir fluid in the water column is everywhere at boiling temperature down to the 370°C isotherm. Whereas this condition at Ohaaki cannot be proven without further drilling, this seems likely as it provides a natural, self-adjusting control on convective heat flow over a shallow

intrusive (cf. Hayba and Engebritsen, 1995; White and Christenson, 2000). Above 370°C, fluid temperatures and pressures would become increasingly influenced by lithostatic confining pressures in silica-rich rocks (Fournier, 1999), as observed in Kakkonda granite (Tosha et al., 2000). Under these conditions the temperature gradients are conductive, with gradients as steep as 33°C/100 m.

Another means of estimating the minimum depth to the BPT zone can be obtained from the ^{13}C equilibrium fractionation kinetics between CH_4 and CO_2. As stated previously, the $\delta^{13}C$ signatures for CO_2 and CH_4 imply equilibrium temperatures on the East Bank ranging between 400°C and 430°C. The fact that CH_4 is not a major gas species in volcanic discharges suggests that both chemical and isotopic equilibration would take place in the aqueous environment either within, or adjacent to, the BPT zone. The reaction rates for both chemical and isotopic equilibration are strongly temperature-dependent (Giggenbach, 1997), with a half-time rate expression for chemical equilibrium of

$$\log t_h = -6.69 + 4440/T\ (\mathrm{K})$$

with the estimated rate of isotopic equilibration for the exchange reaction

$$^{13}CO_2 + {}^{12}CH_4 \Leftrightarrow {}^{12}CO_2 + {}^{13}CH_4$$

some 400 times slower than that for chemical equilibration.

The rate of convective upflow depends on the porosity and the heat input, which in turn controls the vapour–liquid saturation state of the fluid. A conservative heat transfer rate of 10 W/m adjacent to the postulated intrusion yields a darcy velocity of ca. 0.5×10^{-7} (S. White, personal communication, 2000). Assuming a bulk porosity of 10% for the host greywacke, this leads to a flow velocity of ca. 16 m/yr (White, 1995). With a half-time for the ^{13}C exchange reaction at 430°C of ca. 170 yr, in order to retain the 430°C signature, the fluids would have moved no more than 2700 m. Noting that the production wells on the East Bank produce from between 1100 and 1400 m (Fig. 3), this suggests that the depth of the 430°C isotherm (and the BPT boundary) is between 3800 m and 4100 m, which agrees reasonably closely with the values estimated from boiling-point–depth considerations.

It should be stressed that depths calculated in this fashion are sensitive to both the heat flow and porosity parameters chosen for the calculations, and as such are indicative only. For example, if heat flow is doubled to 20 W/m^2 at 10% porosity, the depth to the BPT increases to ca. 8 km. If the porosity is halved at the original energy flow of 10 W/m^2, the calculated depth to the 430°C isotherm is 5.4 km. Fitting energy flow and porosity to measured field parameters is beyond the scope of this paper; however, the values chosen for the above parameters result in flow velocities that are broadly representative of such systems (e.g. Hayba and Engebritsen, 1995).

From these calculations, we suggest that a late-Quaternary intrusive (perhaps similar to the quartz diorite encountered at Ngatamariki), is situated at a minimum depth at around 4 km depth on the East Bank.

5.2. Near-source environment and processes

As noted previously, the stable isotope data for the Ohaaki discharge water indicate that the convectively circulating fluids in the system are predominantly meteoric. The ca. 20% magmatic component in the discharges probably derives from magmatic vapour which periodically discharges across the BPT into overlying meteoric circulation. The periodicity of breaching of the BPT by magmatic vapour will be a complex function of fluid pressure within the BPT zone, magma movement, strain rate and tectonism (Fournier, 1999). Pressure fluctuations associated with the breaching, on the other hand, will lead to rapid sealing of the failed zones by quartz (Mroczek and Christenson, 2000), thus prescribing a cyclic process. The transient flows of heat and gas into the convecting fluids overlying the BPT zone will cause fluctuations in the vapour–liquid saturation properties of the fluid, but as stated previously, the temperature–depth relationship will be bound by

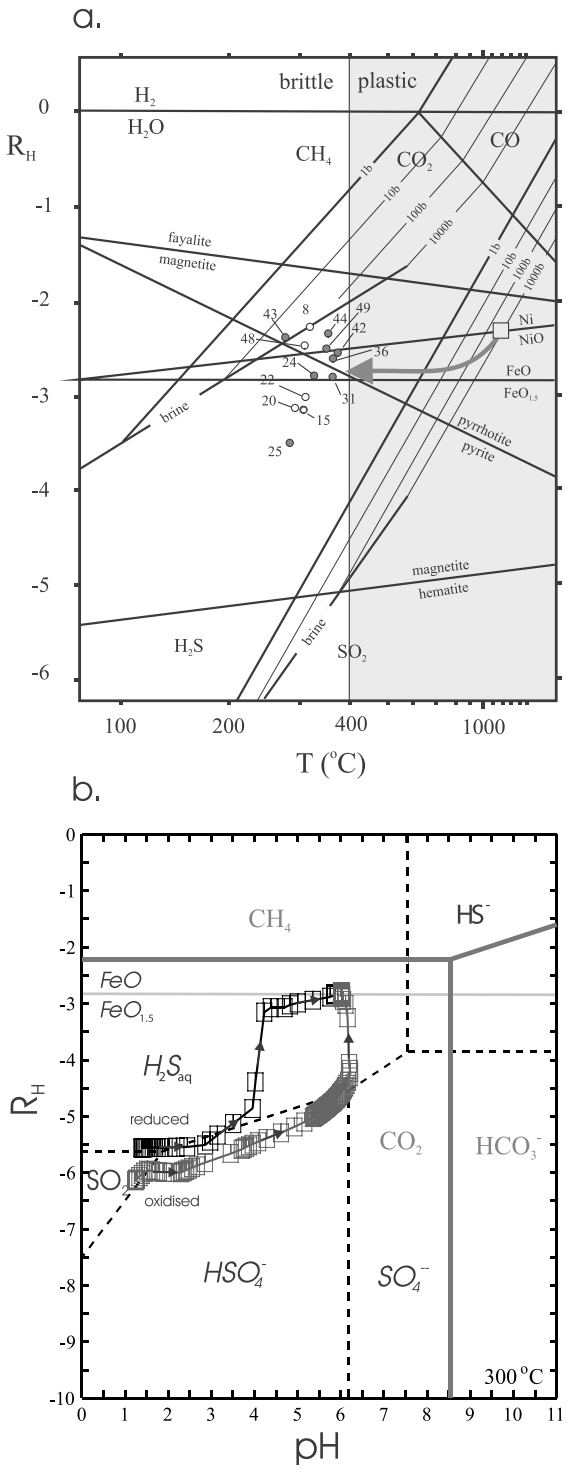

Fig. 19. (a) R_H vs. T_{HA}. Arrow shows possible cooling path for magmatic source components in Ohaaki discharges. (b) R_H vs. pH plot with reaction path traces for titration of greywacke into oxidised and reduced magmatic condensate at 300°C.

the saturated vapour pressure of the water–gas mixture.

An interesting finding of this study is that CO_2 and CH_4 appear to equilibrate at temperatures above that of the BPT. This does not necessarily imply equilibration under supercritical conditions, but raises the more likely scenario that equilibration takes place within the conductively heated region adjacent to the crystallising magma, and in the presence of the high-salinity brine accumulation (e.g. Fournier, 1999). The possible redox–temperature pathway that these fluids might follow is portrayed in Fig. 19a (modified from Giggenbach, 1987).

The initial redox state of the arc-type source melt is likely to be regulated by the Ni–NiO buffer (e.g. Gill, 1981; Luhr, 1992). Cooling of this melt will invariably lead to exsolution of a supercritical aqueous-rich vapour, the redox state for which will be influenced by competing buffers in the respective vapour and melt phases. In the event of a rapid breaching of the magma chamber, such as might occur in a volcanic eruption, the SO_2–H_2S buffer will control the redox state of the fluid phase (Giggenbach, 1987). If, on the other hand, the fluids are trapped into fluid accumulations within the BPT zone, the redox state of the fluid will become increasingly dominated by the FeO–$FeO_{1.5}$ 'rock' buffer, and with further cooling, the fluid composition will shift toward the CH_4–CO_2 buffer, as indicated in Fig. 19a. As the fluid cools, it will eventually reach critical point conditions for its respective bulk salinity, and with further cooling it will generate a high-density brine phase and a low-density, volatile-rich phase. The ^{13}C isotopic evidence suggests that the volatile-rich phase formed in this manner adjacent to the East-Bank heat source is CH_4-bearing, and that this gas periodically breaches the BPT zone to enter into the overlying convecting reservoir.

The Ohaaki data are plotted in Fig. 19a at their

respective H_2/Ar equilibrium temperatures. The H_2/Ar temperatures are everywhere higher than the measured temperatures, pointing to the preservation of higher-temperature equilibrium conditions. The East-Bank values approach the BPT temperature, and are higher than those observed on the West Bank, similar to the relationships observed for ^{13}C fractionation. Although there is some scatter in the data, most discharges plot between the FeO–$FeO_{1.5}$ and CH_4–CO_2 (brine) buffers.

The relationship between redox potential and the ability of the magmatic source fluids to promote hydrolysis reactions is shown in Fig. 19. Here the traces of two reaction path calculations simulating the interaction between two magmatic volatile condensates (one oxidised, one reduced) and greywacke reservoir rocks are plotted in pH–R_H (i.e. $\log(f_{H_2}/f_{H_2O})$) space. The calculations have been made for 300°C using the reaction path code REACT (Bethke, 1992). The bulk fluid composition comprises 1.0 kg of the inferred magmatic gas from White Island (Giggenbach and Sheppard, 1989) condensed into 7 kg water at 300°C, and the greywacke composition is from core retrieved from the Ohaaki field (Palmer et al., 1995). The 'oxidised' fluid in the model is essentially the inferred White Island composition with a total S content of 1.8 mol%, and a SO_2:H_2S mole ratio of 75:25. The reduced fluid is the same bulk composition, but has a SO_2:H_2S mole ratio of 5:95.

The role of sulphur species in controlling the redox state and pH of the fluids is readily apparent. Both condensates are initially in equilibrium with SO_2, but through reaction with FeO in the greywacke and associated acid neutralisation reactions with silicate minerals, the fluid composition migrates along the H_2S_{aq}–HSO_4^- buffer towards increasing pH. When the last of the oxyanions of S are consumed, the path diverts directly toward the FeO–$FeO_{1.5}$ buffer, and it is only at this point where significant quantities of CH_4 begin to be produced. The pH at which CH_4 is initially produced is dependent on the (HCl+HF)/SO_2 ratio of the volatile mix, with the relatively reduced starting fluid generating CH_4 at lower pH than its oxidised counterpart. Although the simulation temperature of 300°C is significantly lower than that inferred for the BPT zone, which has obvious implications for the characteristics of the solvent (e.g. acids being less dissociated at higher temperature), this does not significantly affect the relationship between sulphur reduction, hydrolysis capability of the fluid and generation of CH_4.

The previous discussion leads us to conclude that the condensed magmatic–meteoric fluid mixture residing above the BPT at Ohaaki will be fairly reduced, and not strongly acidic. The reaction path modelling shows that at 300°C and a pH of 4.4, this fluid is in equilibrium with quartz, magnetite, chlorite and the Mg-fluoride mineral hercynite. With further acid neutralisation (to pH 5.5), this assemblage gives way to muscovite, biotite, quartz, magnetite and rhodocrosite. At these higher pH values, any significant pressure transients will lead to rapid partitioning of CO_2 from solution, increased pH and the deposition of calcite (e.g. Simmons and Christenson, 1994). Hence, production of fluids from this environment would certainly lead to calcite scaling in both wells and formation.

5.3. Reservoir model

A geological and geochemical reservoir model which is consistent with the above findings is shown in Fig. 20. Drawn at the same scale as Fig. 3, it shows a small intrusive body under the East-Bank production field at a depth of approximately 4000 m. As discussed above, the reservoir is expected to be two-phase (vapour–liquid) down to the BPT zone, which here is shown to encompass a temperature range of 370–400°C. From the above calculations, the depth to the BPT zone could be as shallow as 3500 m. Heat and mass transfer across the BPT zone and conductive heat flow drive convection above the intrusive, with flow channelled through fault zones which bound the small horst block under the East Bank.

The other main upwelling for the field is assumed to derive from an older and/or deeper intrusive heat source. That this fluid contains more Cl than its younger, shallower neighbour to the east is consistent with the older heat source hav-

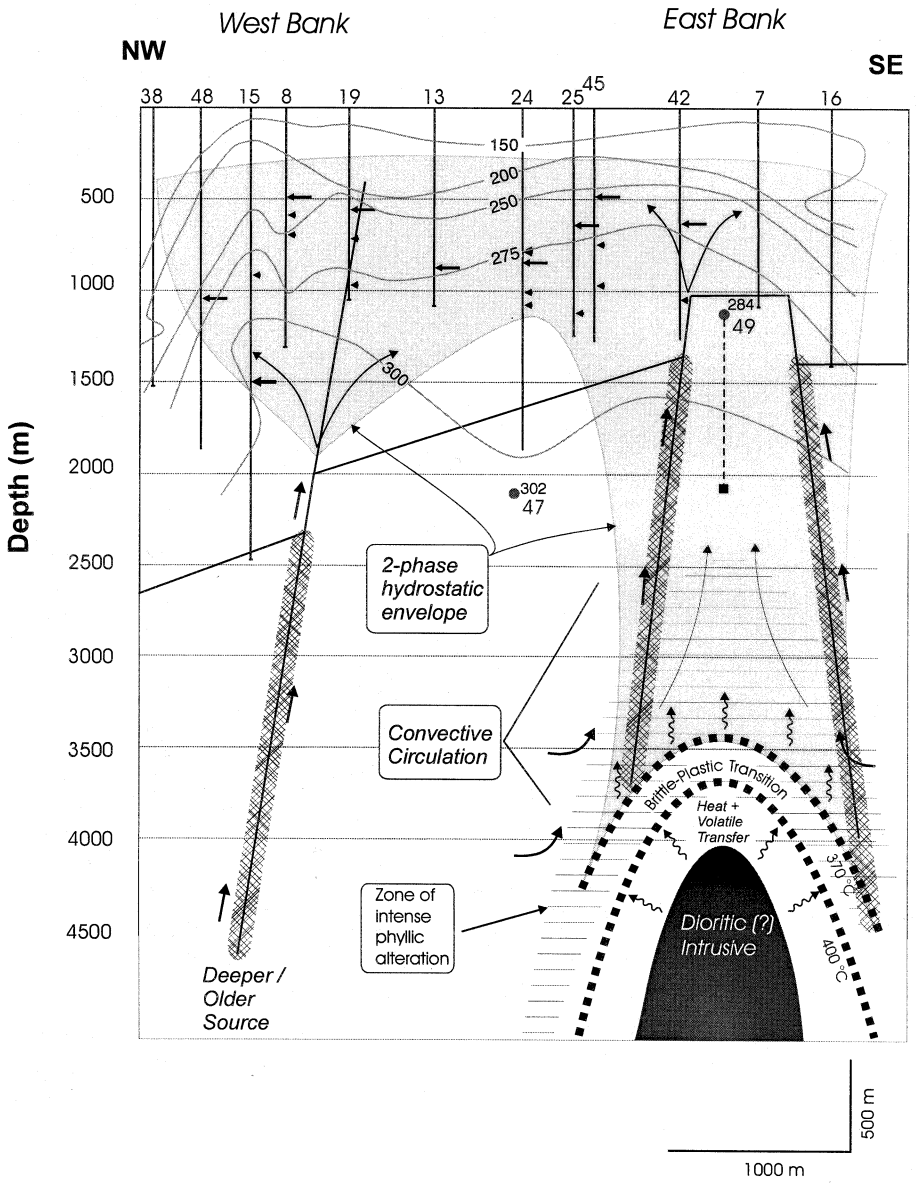

Fig. 20. Reservoir model for the Ohaaki geothermal field.

ing cooled sufficiently to have exposed, through brittle fracturing, its high-salinity brines to convecting meteoric waters. Thus the high-salinity fluids are being flushed from the system as observed at Ngatamariki (Christenson et al., 1998). Such a process would also account for the close similarities in the heaviest observed signatures for $\delta^{18}O$ and $\delta^{2}H$ in water from both production fields.

As stated previously, the presence of a young, shallow intrusive on the East Bank is most consistent with the observed gas signatures from the two production fields, particularly the N_2/Ar and the CO_2/He ratios, but it can also account for the

B and F enrichment in the East-Bank discharges via direct volatile transport and enhanced water–rock interaction processes.

The apparent enrichment of radiogenic gases in the East-Bank discharges is also accounted for in this model. Noting that the gases from both production fields have arc-type magmatic characteristics, and given the close proximity of West-Bank MORB-like $^{3}He/^{4}He$ signatures to the relatively depleted ^{3}He signatures in the east, there is little to suggest that the differences are related to deep-seated (i.e. subduction zone) crustal processes. Rather, it is more likely that the signatures reflect assimilation of crustal material which has not been previously degassed, or perhaps as an extension of this process, that the release of radiogenic gases through hydrothermal alteration of greywacke adjacent to the intrusion. Both explanations are consistent with the views of Stern (1987) who suggests an eastward migration of the arc magmatism through time. In this case, the release of radiogenic gases on the East Bank might best be considered as a short-lived effect.

Acknowledgements

We thank Contact Energy for providing access to the field, advice on the reservoir characteristics, and for valuable logistical support. We are grateful to Pat Browne and Fraser Goff for their thorough reviews of the manuscript, and to Peter Wood and Stephen White for thoughtful discussions during this project. Karen Britten, Mike Crump, Marshall Muller, Ann Noddings are acknowledged for assistance in the field and with analyses. This work was funded by NZ FRST Grant CO5X0004.

References

Bethke, C., 1992. The Geochemists Workbench: A User's Guide to Rxn, Act 2, Tact, React and Gt plot. University of Illinois, Urbana, IL, 213 pp.

Blattner, P., 1985. Isotope shift data and the natural evolution of geothermal systems. Chem. Geol. 49, 187–203.

Browne, P.R.L., Graham, I.J., Parker, R.J., Wood, C.P., 1992. Subsurface andesite lavas and plutonic rocks in the Rotokawa and Ngatamariki geothermal systems, Taupo Volcanic Zone, New Zealand. J. Volcanol. Geotherm. Res. 51, 199–215.

Christenson, B.W., 1997. Kawerau Geothermal Field: Geochemical structure of the reservoir and its response to exploitation. Geotherm. Resour. Counc. Trans. 21, 17–24.

Christenson, B.W., 1989. Fluid inclusion and stable isotope studies in the Kawerau Hydrothermal System, New Zealand: Evidence for past magma–fluid interaction in the active system. IAGC WRI-6 Proceedings, Balkema, Rotterdam, pp. 155–158.

Christenson, B.W., Wood, C.P., 1993. Evolution of a vent-hosted hydrothermal system beneath Ruapehu Crater Lake, New Zealand. Bull. Volcanol. 55, 547–565.

Christenson, B.W., Wood, C.P., Arehart, G.B., 1998. Shallow magmatic degassing: Processes and PTX constraints for paleo-fluids associated with the Ngatamariki diorite intrusion, New Zealand. In: Arehart, G.B., Hulston, J.R. (Eds.), Proceedings of the 9th International Symposium on Water–Rock Interaction. Balkema, Rotterdam, pp. 435–439.

Christenson, B.W., 2000. Geochemistry of fluids associated with the 1995/96 eruption of Mt. Ruapehu, New Zealand: Signatures and processes in the magmatic–hydrothermal system. J. Volcanol. Geotherm. Res. 97, 1–30.

Cole, J.W., 1990. Structural control and origin of volcanism in the Taupo Volcanic Zone, NZ. Bull. Volcanol. 52, 445–459.

Doi, N., Kato, O., Ikeuchi, K., Komatsu, R., Miyazaki, S.I., Akaku, K., Uchida, T., 1998. Genesis of the plutonic–hydrothermal system around Quaternary granite in the Kakkonda geothermal system, Japan. Geothermics 27, 663–690.

Donnelly-Nolan, J.M., Burns, M.G., Goff, F.E., Peters, E.K., Thompson, J.M., 1993. The Geysers–Clear Lake Area, California: Thermal waters, mineralisation, volcanism and geothermal potential. Econ. Geol. 88, 301–316.

Ellis, A.F., Mahon, W.A.J., 1964. Natural hydrothermal systems and experimental hot-water/rock, interactions. Geochim. Cosmochim. Acta 28, 1323–1357.

Ellis, A.J., Sewell, J.R., 1963. Boron in waters and rocks of New Zealand hydrothermal areas. N.Z. J. Sci. 6, 589–606.

Fournier, R.O., 1999. Hydrothermal processes related to movement of fluid from plastic into brittle rock in the magmatic–epithermal environment. Econ. Geol. 94, 1193–1212.

Giggenbach, W.F., 1974. The chemistry of Crater Lake, Mt Ruapehu (New Zealand) during and after the 1971 active period. N.Z. J. Sci. 17, 33–45.

Giggenbach, W.F., 1980. Geothermal gas equilibria. Geochim. Cosmochim. Acta 44, 2021–2032.

Giggenbach, W.F., 1987. Redox processes governing the chemistry of fumarolic gas discharges from White Island, New Zealand. Appl. Geochem. 2, 143–161.

Giggenbach, W.F., Goguel, R.L., 1989. Collection and analysis of geothermal and volcanic water and gas discharges. DSIR Chem. Div. Rep. CD2401, pp. 1–81.

Giggenbach, W.F., 1989. The chemical and isotopic position of the Ohaaki Field within the Taupo Volcanic Zone. Proceedings of the 11th NZ Geothermal Workshop, pp. 81–88.

Giggenbach, W.F., Sheppard, D.S., 1989. Variations in tem-

perature and chemistry of White Island fumarole discharges 1972–1985. N.Z. Geol. Surv. Bull. 103, 119–126.

Giggenbach, W.F., 1991. Chemical techniques in geothermal exploration. In: D'Amore, F. (Ed.), Application of Geochemistry in Geothermal Reservoir Development. UNITAR-UNDP.

Giggenbach, W.F., 1992. Isotopic shifts in waters from geothermal and volcanic systems along convergent plate boundaries and their origin. Earth Planet. Sci. Lett. 113, 495–510.

Giggenbach, W.F., 1995. Variations in the chemical and isotopic composition of fluids discharged over the Taupo Volcanic Zone, New Zealand. J. Volcanol. Geotherm. Res. 68, 89–116.

Giggenbach, W.F., 1997. Relative importance of thermodynamic and kinetic processes in governing the chemical and isotopic composition of carbon-gases in high heat flow sedimentary basins. Geochim. Cosmochim. Acta 61, 3763–3785.

Gill, J.B., 1981. Orogenic Andesites and Plate Tectonics. Springer, Berlin, 390 pp.

Glover, R.B., 1988. Boron distribution between liquid and vapour in geothermal fluids. Proceedings of the 10th New Zealand Geothermal Workshop, pp. 223–229.

Glover, R.B., Hedenquist, J.W., 1989. A brief history of chemical exploration at Ohaaki–Broadlands. Proceedings of the 11th New Zealand Geothermal Workshop, Auckland University, pp. 73–79.

Grant, M.A., 1977. Broadlands – A gas dominated geothermal field. Geothermics 6, 9–29.

Hayba, D.O., Engebritsen, S.I., 1995. Multiphase groundwater flow near cooling plutons. J. Geophys. Res. 102, 12235–12252.

Hedenquist, J.W., Stewart, M.K., 1985. Natural CO_2-rich steam-heated waters in the Broadlands–Ohaaki geothermal system, New Zealand. Their chemistry, distribution and corrosive nature. Trans. Geotherm. Resour. Counc. 9, 245–250.

Hedenquist, J.W., Browne, P.R.L., 1989. The evolution of the Waiotapu geothermal system, New Zealand, based on the chemical and isotopic composition of its fluids, minerals and rocks. Geochim. Cosmochim. Acta 53, 2235–2257.

Hedenquist, J.W., 1990. The thermal and geochemical structure of the Broadlands–Ohaaki geothermal system, New Zealand. Geothermics 19, 151–185.

Hulston, J., Lupton, J., 1996. Helium isotope studies of geothermal fields in the Taupo Volcanic Zone, New Zealand. J. Volcanol. Geotherm. Res. 74, 297–321.

Hulston, J.R., Taylor, C.B., Lyon, G.L., Stewart, M.K., Cox, M.A., 1981. Environmental isotopes in New Zealand hydrology. Part 2. Standards, measurement techniques and reporting of measurements of oxygen-18, deuterium and tritium in water. N.Z. J. Sci. 24, 313–322.

Kennedy, B.M., Lynch, M.A., Reynolds, J.H., Smith, S.P., 1985. Intensive sampling of noble gases in fluids at Yellowstone, I. Early overview of the data; regional patterns. Geochim. Cosmochim. Acta 49, 1241–1261.

Kennedy, B.M., Truesdell, A.H., 1996. The northwest Geysers high temperature reservoir: Evidence for active magmatic degassing and implications for the origin of the Geysers Geothermal Field. Geothermics 25, 365–387.

Kissling, W.M., 1997. Large scale hot plate models for the TVZ geothermal fields. Proceedings of the 19th New Zealand Geothermal Workshop, Auckland University, pp. 51–56.

Luhr, J.F., 1992. Slab-derived fluids and partial melting in subduction zones: insights from two contrasting Mexican volcanoes (Colima and Ceboruco). J. Volcanol. Geotherm. Res. 54, 1–18.

Lyon, G.L., Hulston, J.R., 1984. Carbon and hydrogen isotopic compositions of New Zealand geothermal gases. Geochim. Cosmochim. Acta 48, 1161–1171.

Mahon, W.A.J., Finlayson, J.B., 1977. The chemistry of the Broadlands geothermal area, New Zealand. Am. J. Sci. 272, 48–68.

Marty, B., Jambon, A., 1987. C/^{3}He in volatile fluxes from the solid Earth: implications for carbon geodynamics. Earth Planet. Sci. Lett. 83, 16–26.

McNabb, A., 1992. The Taupo–Rotorua hot-plate. Proceedings of the 14th New Zealand Geothermal Workshop, Auckland University, pp. 111–114.

Mroczek, E.K., Christenson, B.W., 2000. Solubility of quartz in hypersaline brine – Implications for fracture permeability in magma-ambient environments. Proceedings 2000 World Geothermal Congress, pp. 1459–1462.

Muraoka, H., Uchida, T., Sasada, M., Yagi, M., Akaku, K., Sasaki, M., Yasukawa, K., Miyazaki, S., Doi, N., Saito, S., Sato, K., Tanaka, S., 1998. Deep geothermal resources survey program: Metamorphic and hydrothermal processes in a well encountering 500°C at 3729 m depth, Kakkonda, Japan. Geothermics 27, 507–534.

Nishio, Y., Sasaki, S., Gamo, T., Hiyagon, H., Sano, Y., 1998. Carbon and helium isotope systematics of North Fihi Basin basalt glasses: carbon geochemical cycle in the subduction zone. Earth Planet. Sci. Lett. 62, 239–257.

Palmer, K., Mortimer, N., Nathan, S., Isaac, M.J., Field, B.D., Sircombe, K.N., Black, P.M., Bush, S., Orr, N.W., 1995. Chemical and petrographic analyses of some New Zealand Paleozoic–Mesozoic metasedimentary and igneous rocks. IGNS Sci. Rep. 95/16.

Quisefit, J.P., Toutain, J.P., Bergametti, G., Javoy, M., Cheynet, B., Person, A., 1989. Evolution versus cooling of gaseous volcanic emissions from Momotombo Volcano, Nicaragua: Thermochemical model and observations. Geochim. Cosmochim. Acta 53, 2591–2608.

Reyes, A.G., Vickridge, I.C., 1996. Distribution of lithium, boron and chloride between fresh and altered rocks in the Kawerau geothermal system, New Zealand. Proceedings of the 18th NZ Geothermal Workshop, Auckland University, pp. 121–126.

Risk, G.F., 1993. Resurvey of resistivity boundary of Ohaaki Geothermal Field, 1975–1993. Proceedings of the 15th NZ Geothermal Workshop, pp. 195–200.

Sano, Y., Marty, B., 1995. Origin of carbon in fumarolic gas from island arcs. Chem. Geol. 119, 265–274.

Simmons, S.F., Browne, P.R.L., 2000. Hydrothermal minerals

and precious metals in the Broadlands–Ohaaki geothermal system: Implications for understanding low-sulfidation epithermal environments. Econ. Geol. 95, 971–999.

Simmons, S.F., Christenson, B.W., 1994. Origins of calcite in a boiling geothermal system. Am. J. Sci. 294, 361–400.

Stern, T.A., 1987. Asymmetric back-arc spreading, heat flux and structure associated with the Central Volcanic Region of New Zealand. Earth Planet. Sci. Lett. 85, 265–276.

Stewart, M.K., 1978a. Isotope measurements at Broadlands. Geotherm. Circ. MKS-2, INS Contrib. 882.

Stewart, M.K., 1978b. Stable isotopes in waters from the Wairakei geothermal system, New Zealand. N.Z. DSIR Bull. 220, 399–412.

Stewart, M.K., 1992. Environmental isotope survey of Ohaaki geothermal waters in 1990. DSIR Rep. DSIRPS-C-60.

Sutton, F.M., McNabb, A., 1977. Boiling curves at Broadland geothermal field, New Zealand. N.Z. J. Sci. 20, 333–337.

Taran, Y.A., Pokrovsky, B.G., Esikov, A.D., 1989. Deuterium and oxygen-18 in fumarolic steam and amphiboles from some Kamchatka volcanoes: 'andesitic waters'. Dokl. Akad. Nauk USSR 304, 440–443.

Tosha, T., Koide, K., Ohminato, T., Akaku, K., Doi, N., 2000. Recent results of 'Deep-seated geothermal resources survey' project in the Kakkonda geothermal field, Japan. Proceedings 2000 World Geothermal Congress, pp. 1877–1882.

Wardell, L.J., Kyle, P.R., Dunbar, N., Christenson, B.W., 2001. White Island volcano, New Zealand: Carbon dioxide and sulfur dioxide emission rates and melt inclusion studies. Chem. Geol. 177, 187–200.

Weir, G., 2000. A mathematical model coupling heat and mass flow and extension rate in the Taupo Volcanic Zone, New Zealand. Proceedings 2000 World Geothermal Congress, pp. 889–893.

White, S., 1995. Multiphase nonisothermal transport of chemical systems. Water Resour. Res. 31, 1761–1772.

White, S., Christenson, B.W., 2000. Modelling the alteration associated with diorite intrusions. Proceedings 2000 World Geothermal Congress, pp. 3969–3974.